People`s Democratic Republic of Algeria

Ministry of Higher Education and Scientific Research

University of Echahid Hamma Lakhdar - El Oued

Faculty of Technology

Department of Electrical Engineering

Dissertation

ACADEMIC MASTER

Division: Electrical Engineering

Specialty: Electrical networks

Presented by:

- **HADJ AMMAR Rami**
- **BEGGAS Riadh**

Entitled:

Optimizing High Voltage Insulator Surface Design for Improved Electrical Performance

Dissertation Submitted in Partial Fulfilment of the Requirements for the Master

Board of Examiners:

Academic Year: 2024/2025


بسم الله الرحمن الرحيم

Acknowledgement

first of all, we hold our thanks to ***ALLAH*** *for giving us strength and courage*

following we would like to warmly thank ***Dr. Guia Talal*** *our supervisor who has made enormous effort through his information,*

and all ***the professors of the department*** *of electrical engineering to all those who were at one time or at any time involved in this work,*

our warmest thanks to all those who from near and far have contributed to the realisation of this thesis

Dedicate

we dedicate this modest thesis to ***our parents*** *who were able to support us through our studies, and who without them we could not have done this work*

we dedicate this modest work:

to our ***brothers*** *and* ***sisters***

to our ***family*** *'s*

to all our ***loyal friends***

our dedication also goes to those who have participated directly or indirectly in the culmination of our effort

الملخص:

عنوان المذكرة: تحسين تصميم سطح العوازل الكهربائية ذات الجهد العالي لتحسين الأداء الكهربائي
الكلمات المفتاحية: العوازل الكهربائية ذات الجهد العالي، التشكيل السطحي، خاصية كره الماء، مقاومة التلوث، جهد الانهيار، التنظيف الذاتي، توزيع المجال الكهربائي، هندسة الأسطح.
الملخص:

تلعب العوازل الكهربائية ذات الجهد العالي دورًا حيويًا في أنظمة الطاقة الكهربائية، لكن أداءها غالبًا ما يتأثر بالتلوث البيئي والرطوبة وتدهور السطح. وقد ظهرت تقنية التشكيل السطحي كنهج مبتكر لتحسين أداء العوازل من خلال تعزيز خاصية كره الماء، ومقاومة التلوث، وزيادة جهد الانهيار. يستعرض هذا البحث التقدمات الحديثة في تقنيات التشكيل السطحي بما في ذلك النقش بالليزر، المعالجة بالبلازما، الهياكل المجهرية المصبوبة، التصاميم المستوحاة من الطبيعة، والتصنيع بالإضافة، وتأثيرها على كفاءة العوازل. تُظهر الدراسات أن الأسطح المهندسة يمكن أن تقلل من تراكم الملوثات، وتعزز سلوك التنظيف الذاتي، وتحسّن توزيع المجال الكهربائي، مما يساهم في إطالة عمر الخدمة وتحسين الموثوقية. ومع ذلك، لا تزال هناك تحديات مثل المتانة طويلة الأمد، وقابلية التطبيق على نطاق واسع، وتوحيد المعايير، والتي تتطلب المزيد من البحث. من خلال تحليل الأساليب الحالية ونتائج الأداء، يسلط هذا العمل الضوء على إمكانيات التشكيل السطحي كحل فعال من حيث التكلفة لعوازل الجهد العالي من الجيل القادم في البيئات التشغيلية القاسية.

Abstract:

Thesis title: Optimizing High Voltage Insulator Surface Design for Improved Electrical Performance
Keywords: High-voltage insulators, Surface texturing, Hydrophobicity, Pollution resistance, Flashover voltage, Self-cleaning, Electric field distribution.
Abstract:

High-voltage insulators play a critical role in electrical power systems, but their performance is often compromised by environmental pollution, moisture, and surface degradation. Surface texturing has emerged as an innovative approach to enhance insulator performance by improving hydrophobicity, pollution resistance, and flashover voltage. This review examines recent advancements in surface texturing techniques including laser ablation, plasma treatment, molded microstructures, bio-inspired designs, and additive manufacturing and their impact on insulator efficiency. Studies demonstrate that engineered surface textures can reduce contamination accumulation, promote self-cleaning behavior, and optimize electric field distribution, thereby extending service life and reliability. However, challenges such as long term durability, scalability, and standardization remain areas for further research. By analyzing existing methodologies and performance outcomes, this work highlights the potential of surface texturing as a cost effective solution for next generation high voltage insulators in demanding operational environments.

CONTENTS

Contents

LIST OF ABBREVIATIONS AND SYMBOLS III

LIST OF FIGURES IV

LIST OF TABLES VII

GENERAL INTRODUCTION 1

CHAPTER I: GENERAL REVIEW ABOUT HIGH VOLTAGE OUTDOOR INSULATORS 3

I.1 INTRODUCTION 3
I.2 OUTDOOR INSULATORS 3
I.3 INSULATING MATERIALS 3
I.3.1 Ceramic 4
I.3.2 Glass 4
I.3.3 Synthetic (Composite) Materials 5
I.4 INSULATOR AGING 6
I.4.1 Thermal Aging 6
I.4.2 Electrochemical Aging 6
I.5 MAIN TYPES OF INSULATORS : 6
I.5.1 Rigid-Type Insulators: 6
I.5.2 Pin-and-Cap Insulators: 7
I.5.3 Long-Rod Insulators: 11
I.6 INSULATOR POLLUTION 12
I.6.1 Types of Pollution 12
I.6.2 Classification of Pollution Types 13
I.6.3 Insulator Behavior Under Polluted Conditions 15
I.7 CONCLUSION : 17

CHAPTER II: OPTIMIZING HIGH VOLTAGE INSULATOR SURFACE DESIGN USING TEXTURED POLYMERIC INSULATORS 18

II.1 INTRODUCTION: 18
II.2 TEXTURING OF POLYMERIC INSULATORS 18
II.2.1 Surface patterns 19
II.2.2 Power dissipation factor 22
II.2.3 Theoretical classification of candidate textures 23
II.3 INSULATOR PROFILE AND TEXTURES [30] 23
II.3.1 CONVENTIONAL INSULATOR PROFILE 23
II.3.2 TEXTURED-TRUNK (TT) INSULATORS 24
II.4 COMPARATIVE CLEAN-FOG TESTS 28
II.4.1 TEST PROCEDURES 28
II.4.2 MEAN FLASHOVER VOLTAGES (FOV) 28
II.4.3 COMPARISON OF FOV FOR TEXTURED AND CONVENTIONAL INSULATORS 30

II.4.4 FOV VARIATION WITH DEGREE OF POLLUTION 31
II.4.5 FOV VARIATION DURING RAMP TEST SERIES 31
II.5 LEAKAGE CURRENT AND DATA PROCESSING 32
II.5.1 TIME WINDOWS 32
II.5.2 20 ms (SINGLE-CYCLE) WINDOW 33
II.5.3 2 s (100-CYCLE) WINDOW 34
II.6 CONCLUSIONS 41

CHAPTER III: EXPERIMENTAL STUDY AND RESULTS 42

III.1 INTRODUCTION 42
III.2 EXPERIMENTAL SETUP 42
III.2.1 High Voltage Laboratory Test Circuit (University of El Oued) 42
III.3 OPERATING MODE 46
III.3.1 Experimental model 46
III.3.2 Preparation of the model 47
III.4 TEST PROCEDURE 47
III.4.1 Flashover Voltage Measurement 47
III.4.2 Leakage Current Measurement 47
III.4.3 Atmospheric Correction 48
III.5 EXPERIMENTAL RESULTS 49
III.5.1 The non- textured sample [33] 49
III.5.2 A 60 Degree Textured Sample 49
III.5.3 A 45 Degree Textured Sample 51
III.5.4 Longitudinally Textured Sample [33] 52
III.5.5 Transversely Textured Sample [33] 53
III.5.6 Leakage current 54
III.5.7 Final Extraction 62
III.6 CONCLUSION 63

GENERAL CONCLUSION 64

REFERENCES 59

List of Abbreviations and Symbols

List of Abbreviations and symbols

Abbreviation	Definition
HTM	Hydrophobicity Transfer Materials
FOV	Flashover Voltages
EPDM	Ethylene Propylene Diene Monomer
CONV	Conventional
TXT	Textured (Insulator)
TT	Textured Trunk
TTS	Textured Trunk And Shed
SDD	Soluble Deposit Density
NSDD	Non-Soluble Deposit Density
PLA+	Plastique (Type Of Polymer)
SIR	Silicone Insulator Rubber

List of Figures and Tables

List of Figures

FIGURE I.1. CERAMIC INSULATOR 4

FIGURE I.2. SYNTHETIC MATERIAL INSULATORS. 5

FIGURE I.3 CROSS-SECTIONAL VIEW OF A GLASS RIGID INSULATOR 7

FIGURE I.4: PIN-AND-CAP INSULATOR 7

FIGURE I.4.A: STANDARD PROFILE PIN-AND-CAP INSULATOR. 8

FIGURE I.4.B: ANTI-FOG PROFILE (TYPE A) PIN-AND-CAP INSULATOR 8

FIGURE I.4.C: FOG-RESISTANT PROFILE (TYPE B) PIN-AND-CAP INSULATOR 9

FIGURE I.4.D: FLAT (AERODYNAMIC) PROFILE PIN-AND-CAP INSULATOR 9

FIGURE I.4.E: SPHERICAL PROFILE PIN-AND-CAP INSULATOR 10

FIGURE I.6: LONG-ROD INSULATORS 11

FIGURE II-1. SIDE VIEW OF PART-SPHERICAL PROTUBERANCE (A) AND TOP VIEW OF AN ARRAY OF CONTIGUOUS PART-SPHERICAL PROTUBERANCES (B) [29]. 20

FIGURE II.2. TEXTURED PATTERNS: CONTIGUOUS HEXAGONAL (A), INTERSECTING HEXAGONAL (B), INTERSECTING SQUARE (C) AND INTERSECTING TRIANGULAR (D) [29]. 22

FIGURE II.3 4MM TEXTURED TRUNK INSULATOR (TT4). CAD IMAGE. 24

FIGURE II.4. HEMISPHERICAL PROTUBERANCES: SQUARE-INTERSECTION GEOMETRY. 25

FIGURE II.5. TTS6 INSULATOR: DETAIL OF THE DOUBLE RIDGE PATTERN OF THE SHED UNDERSIDE AND THE JUNCTION WITH THE SHANK TEXTURE (CAD IMAGE). 26

FIGURE II. 6. LOGARITHMIC SPIRAL OF CONSTANT ANGLE 45°. 27

FIGURE II. 7. MEAN FOV FOR TEXTURED AND CONVENTIONAL INSULATORS. MATERIAL A AND B (DARK AND LIGHT GREY RESPECTIVELY) FOG SPRAY RATE 3 L/HR. TWO SDD LEVELS. 29

FIGURE II.8A. FOV REDUCTION WITH INCREASING SDD (MATERIAL A) FOG SPRAY RATES 3 AND 8 L/H. TXT VALUES ARE MEAN OF TT AND TTS FOVS 31

..... 31

FIGURE II. 9. MEAN FOV OF 6 TEST SERIES FOR TTS4 SILICONE RUBBER INSULATORS. MATERIAL A. EACH SERIES CONSISTS OF 8 RAMP VOLTAGE TESTS. SDD 0.64 MG/CM2. FOG SPRAY RATE 8 L/H. 31

FIGURE II. 8B. FOV REDUCTION WITH INCREASING SDD (MATERIAL B) FOG SPRAY RATES 3 AND 8 L/H. TXT VALUES ARE MEAN OF TT AND TTS FOVS. 32

FIGURE II.10. MEAN FOV OF 6 TEST SERIES FOR TTS4 SILICONE RUBBER INSULATORS. MATERIAL A. EACH SERIES CONSISTS OF 4 RAMP VOLTAGE TESTS. SDD 0.64MG/CM2. FOG SPRAY RATE 3L/H. 32

FIGURE II.11A. RAMP VOLTAGE TEST SERIES FOR TT4A INSULATOR UNDER CONDITIONS OF HIGH POLLUTION (0.64 MG/CM2) AND HIGHER FOG SPRAY RATE (8 L/H). 33

FIGURE II.11B. RAMP 1 OF TEST SERIES FOR TT4A INSULATOR UNDER CONDITIONS OF HIGH POLLUTION (0.64 MG/CM2) AND HIGHER FOG SPRAY RATE (8 L/H). FOV 28.9 KV AT 320 S. 34

FIGURE II.11 C,D. RAMPS 3 AND 8 OF TEST SERIES FOR TT4A INSULATOR UNDER CONDITIONS OF HIGH POLLUTION (0.64 MG/CM2) AND HIGHER FOG SPRAY RATE (8 L/H). RAMP3: FOV 25.2 KV AT 301 S; RAMP8: FOV 39.7 KV AT 520 S. 34

FIGURE II.12A. ANALYSIS (2 S WINDOW) OF RAMP VOLTAGE DATA FOR A TT4 INSULATOR, FOR HIGH POLLUTION (0.64MG/CM2) AND LOWER FOG SPRAY RATE (3L/H) (3RD RAMP). FOV 27 KV AT 340 S. 35

FIGURE II.12B. ANALYSIS (2 S WINDOW) OF RAMP VOLTAGE DATA FOR A TTS4A INSULATOR, FOR HIGH POLLUTION (0.64 MG/CM2) AND LOWER FOG SPRAY RATE (3L/H) (3RD RAMP). FOV 30.6 KV AT 400 S. 37

FIGURE II.12C. ANALYSIS (2 S WINDOW) OF RAMP VOLTAGE DATA FOR A TT6B INSULATOR, FOR HIGH POLLUTION (0.64 MG/CM2) AND LOWER FOG SPRAY RATE (3L/H) (3RD RAMP). FOV 31.4 KV AT 410 S. 38

FIGURE II. 12D. ANALYSIS (2 S WINDOW) OF RAMP VOLTAGE DATA FOR A TTS6B INSULATOR, FOR HIGH POLLUTION (0.64 MG/CM2) AND LOWER FOG SPRAY RATE (3L/H) (3RD RAMP). FOV 32.9 KV AT 372 S. 39

FIGURE II.13. LEAKAGE RESISTANCE DURING A RAMP-VOLTAGE FLASHOVER TEST FOR CONVA AND TSS4A INSULATORS. UPPER CURVE: CONVA. LOWER CURVE: TTS4A. (0.64 MG/CM2, 8 L/H) 2 S SAMPLE WINDOW ANALYSIS. 40

FIGURE III.1. DIGITAL OSCILLOSCOPE. 43

FIGURE III.2. PHOTO OF THE CONTROL PANEL IN THE HIGH VOLTAGE LABORATORY AT THE UNIVERSITY OF EL OUED. 44

FIGURE III.3. INDUSTRIAL FREQUENCY TEST CIRCUIT. 45

FIGURE III. 4. PHOTO OF THE INDUSTRIAL FREQUENCY TEST CIRCUIT. 46

FIGURE III.5. THREE SAMPLES: A TRADITIONAL NON- TEXTURED SAMPLE AND TWO WOVEN SAMPLES 47

FIGURE III .7. REAL IMAGES OF THE FLASHOVER VOLTAGE VARIATION IN THE NON-TEXTURED SAMPLE AT DIFFERENT DISTANCE BETWEEN THE ELECTRODES: (A) 4CM, (B) 8 CM. 49

FIGURE III. 9. REAL IMAGES OF THE FLASHOVER VOLTAGE VARIATION IN 60 DEGREE TEXTURED SAMPLE AT VARYING DISTANCE BETWEEN THE ELECTRODES: (A) 4CM, (B) 8 CM. 50

FIGURE III. 9. REAL IMAGES OF THE FLASHOVER VOLTAGE VARIATION IN 45 DEGREE TEXTURED SAMPLE AT VARYING DISTANCE BETWEEN THE ELECTRODES: (A) 4CM, (B) 8 CM. 51

FIGURE III. 9. REAL IMAGES OF THE FLASHOVER VOLTAGE VARIATION IN THE LONGITUDINALLY TEXTURED SAMPLE AT DIFFERENT DISTANCE BETWEEN THE ELECTRODES : (A) 4CM, (B) 8 CM. 52

FIGURE III.11. REAL IMAGES OF THE FLASHOVER VOLTAGE VARIATION IN THE TRANSVERSELY TEXTURED SAMPLE AT DIFFERENT DISTANCE BETWEEN THE ELECTRODES : (A) 4CM, (B) 8 CM. 53

TABLE III.4. THE TABLE REPRESENTS THE VALUES OF CURRENT LEAKAGE AT DIFFERENT VOLTAGES 54

FIGURE III.14. GRAPHICAL CURVES OF LEAKAGE CURRENT FOR THE NON-TEXTURED SAMPLE UNDER DIFFERENT VOLTAGES: (A) 2KV, (B) 5KV, (C) 8KV. 54

FIGURE III.15. GRAPHICAL CURVES OF LEAKAGE CURRENT FOR THE NON-TEXTURED SAMPLE UNDER DIFFERENT VOLTAGES: (A) 2KV, (B) 5KV, (C) 8KV. 55

TABLE III.4. THE TABLE REPRESENTS THE VALUES OF CURRENT LEAKAGE AT DIFFERENT VOLTAGES 55

FIGURE III.14. GRAPHICAL CURVES OF LEAKAGE CURRENT FOR TEXTURED SAMPLE WITH A 60-DEGREE ANGLE UNDER DIFFERENT VOLTAGES: (A) 2KV, (B) 5KV, (C) 8KV. 56

FIGURE III.14. GRAPHICAL CURVES OF LEAKAGE CURRENT FOR TEXTURED SAMPLE WITH A 60 DEGREE ANGLE UNDER DIFFERENT VOLTAGES: (A) 2KV, (B) 5KV, (C) 8KV. 56

FIGURE III.14. GRAPHICAL CURVES OF LEAKAGE CURRENT FOR TEXTURED SAMPLE WITH A 45 DEGREE ANGLE UNDER DIFFERENT VOLTAGES: (A) 2KV, (B) 5KV, (C) 8KV. 57

FIGURE III.14. GRAPHICAL CURVES OF LEAKAGE CURRENT FOR TEXTURED SAMPLE WITH A 45 DEGREE ANGLE UNDER DIFFERENT VOLTAGES: (A) 2KV, (B) 5KV, (C) 8KV. 58

FIGURE III. 16.GRAPHICAL CURVES OF LEAKAGE CURRENT FOR THE LONGITUDINALLY TEXTURED SAMPLE UNDER DIFFERENT VOLTAGES: (A) 2KV, (B) 5KV, (C) 8KV. 59

FIGURE III.17. GRAPHICAL CURVES OF LEAKAGE CURRENT FOR THE LONGITUDINALLY TEXTURED SAMPLE UNDER DIFFERENT VOLTAGES: (A) 2KV, (B) 5KV, (C) 8KV. 60

FIGURE III.18. GRAPHICAL CURVES OF LEAKAGE CURRENT FOR THE TRANSVERSELY TEXTURED SAMPLE UNDER DIFFERENT VOLTAGES: (A) 2KV, (B) 5KV, (C) 8KV. 61

FIGURE III.19. GRAPHICAL CURVES OF LEAKAGE CURRENT FOR THE TRANSVERSELY TEXTURED SAMPLE UNDER DIFFERENT VOLTAGES: (A) 2KV, (B) 5KV, (C) 8KV. 61

FIGUREIII.20 COMPARISON OF FLASHOVER VOLTAGE AND LEAKAGE CURRENT FOR TEXTURED AND NON-TEXTURED INSULATOR SAMPLES 62

List of Tables

TABLE I-1 CLASSIFICATION OF POLLUTION ACCORDING TO ENVIRONMENTAL TYPE: 14

TABLE II-1. THEORETICAL CLASSIFICATION OF TEXTURED PATTERNS. TABLE ADOPTED FROM [28]. 23

TABLE 1. CREEPAGE DISTANCES FOR CONVENTIONAL AND TEXTURED INSULATORS. 26

TABLE II.3. TEST RESULTS (INCLUDE ONLY THE FIRST 4 RAMPS OF EACH SERIES). 30

TABLE III.1. THE TABLE REPRESENT CHANGES IN VOLTAGE ACROSS THE NON- TEXTURED SAMPLE VARYING DISTANCE BETWEEN THE ELECTRODES. 49

TABLE III.2. THE TABLE REPRESENT CHANGES IN VOLTAGE ACROSS 60 DEGREE TEXTURED SAMPLE AT VARYING DISTANCE BETWEEN THE ELECTRODES. 50

TABLE III.3. THE TABLE REPRESENT CHANGES IN VOLTAGE ACROSS 45 DEGREE TEXTURED SAMPLE AT VARYING DISTANCE BETWEEN THE ELECTRODES. 51

TABLE III.2. THE TABLE REPRESENT CHANGES IN VOLTAGE ACROSS LONGITUDINALLY TEXTURED SAMPLE AT VARYING DISTANCE BETWEEN THE ELECTRODES. 52

TABLE III.3. THE TABLE REPRESENT CHANGES IN VOLTAGE ACROSS TRANSVERSELY TEXTURED SAMPLE AT VARYING DIMENSION BETWEEN THE ELECTRODES. 53

TABLE III.4. THE TABLE REPRESENTS THE VALUES OF CURRENT LEAKAGE AT DIFFERENT VOLTAGES 57

TABLE III.5. THE TABLE REPRESENTS THE VALUES OF CURRENT LEAKAGE AT DIFFERENT VOLTAGES 58

TABLE III.6. TABLE III.6. THE TABLE REPRESENTS THE VALUES OF CURRENT LEAKAGE AT DIFFERENT VOLTAGES. 60

GENERAL INTRODUCTION

General Introduction

High voltage insulators play a fundamental role in modern electrical power systems by ensuring the safe and efficient transmission and distribution of electricity. These specialized components are designed to withstand extremely high voltages while providing reliable electrical insulation and mechanical support for conductors, preventing unwanted current leakage or short circuits [1]. Their primary function is to isolate live electrical parts from grounded structures, such as transmission towers, poles, or substation equipment, while also enduring various environmental and operational stresses [2].

The importance of high voltage insulators becomes evident in their widespread use across power networks, including overhead transmission lines, distribution systems, and substation installations [3]. They must maintain their insulating properties under diverse conditions, such as heavy rain, pollution, extreme temperatures, and mechanical loads caused by wind or ice. Over time, different materials have been developed to enhance their performance, including traditional porcelain, toughened glass, and modern polymer composites, each offering distinct advantages in terms of durability, weight, and resistance to environmental factors [4].

In addition to their electrical and mechanical functions, high voltage insulators contribute to the overall stability of power grids by minimizing energy losses and preventing faults that could lead to outages [1]. Their design and material selection are critical, as they must balance high dielectric strength with long-term reliability. As power systems evolve with higher voltages and more demanding operating conditions, ongoing research and innovation in insulator technology continue to improve their efficiency and lifespan [5]. The proper selection, installation, and maintenance of these insulators are essential for ensuring the uninterrupted supply of electricity in both industrial and residential applications [2].

Our objective is to improve the performance of composite insulators for high voltages. In order to conduct this study properly, we have divided our work into three chapters.

In the first chapter, we will discuss high-voltage insulators and their types, as well as define the phenomenon of pollution affecting high-voltage insulators and the different types of pollution.

In the second chapter, we will address the methods for improving the performance of high-voltage insulators.

In the third chapter, we will examine experiments conducted on two plastic samples using a two different textured surface patterns and compare it to the previous studies

CHAPTER I

GENERAL REVIEW ABOUT HIGH VOLTAGE OUTDOOR INSULATORS

Chapter I: General review about high voltage outdoor insulators

I.1 Introduction

For technical and economic reasons, the transmission and distribution of electrical energy are generally carried out at high voltage (primarily via overhead lines, but also through underground cables). The reliability of energy transmission depends significantly on the long-term mechanical, electrical, and dielectric behavior of the various components of lines and substations. Among these components, insulators play a fundamental role. In most high voltage power lines, insulators are threatened by the phenomenon of pollution [6].

This chapter focuses on high voltage insulators, their various types, as well as the materials used in their manufacture. We then address the phenomenon of pollution in general and its harmful effects on the behavior of insulators.

I.2 Outdoor Insulators

The demand for electrical energy has been gradually increasing. To transmit massive amounts of electricity, high voltage transmission systems are extensively used. In transmission systems, high voltage apparatus such as insulators play a crucial role in ensuring normal power supply operation [7].

Outdoor insulators are widely used in power transmission and distribution networks. They provide mechanical support to overhead line conductors and electrically isolate them from the tower. This section provides insight into three different insulating materials used today: porcelain, glass, and polymers. Porcelain and glass are also called ceramic insulators, while polymer insulators are known as composite or non-ceramic insulators. Different insulator profiles are selected based on environmental conditions and their intended application, such as suspension, tension, and post types. Insulators are also available in various dimensions and designs according to voltage rating [8, 9].

I.3 Insulating Materials

Several solid insulating materials can be used for manufacturing high-voltage insulators, including glass, ceramic, and porcelain. However, in recent years, porcelain has been increasingly abandoned due to two main disadvantages: the heavy weight of porcelain insulators and the

difficulty in detecting partial discharges. In recent times, there has been growing interest in using polymer material insulators [10, 11].

I.3.1 Ceramic

The development and manufacturing of ceramics date back a long time due to their excellent performance. For insulators installed in locations with significant mechanical stresses, fine-grained ceramic is preferably used. Ceramic is commonly found in substations for various applications: support insulators, insulating covers for disconnect switches, circuit breakers, potential transformers, and bushings for power transformers, among others [10, 12].

Figure I.1. *Ceramic Insulator*

I.3.2 Glass

In Algeria, the insulators used in medium and high voltage lines are made of glass. Among the advantages of glass are its low cost and the ease of defect observation [13]. We find two types of glass used in the manufacture of insulators: tempered glass and annealed glass [14].

I.3.2.1 Tempered glass

This is obtained by reheating the insulator removed from the mold to a temperature of about 70°C, then cooling it with jets of pressurized air strategically distributed over its entire surface; the

outer layers of the insulating part quickly acquire a rigidity that prevents any deformation [15]. Tempered glass has a mechanical tensile stress about 5 to 6 times greater than annealed glass and can withstand sudden temperature variations of up to 100°C [15]. The green color of the glass insulator comes from the iron oxide present in its composition - if this is absent, the glass is transparent [15]. Besides its low cost, glass has the advantage of allowing defects to be detected by simple visual inspection [16].

I.3.2.2 Annealed glass

It was mainly used to make rigid insulators, but it was found that somewhat thick insulators could not withstand sudden temperature changes. Moreover, annealed glass can only withstand relatively low mechanical stresses, which prohibits its use for suspension insulators [16].

I.3.3 Synthetic (Composite) Materials

Synthetic composite insulators consist of a resin-impregnated fiberglass core and an elastomer ribbed coating. They offer the advantages of being lightweight while maintaining high mechanical strength. [17]

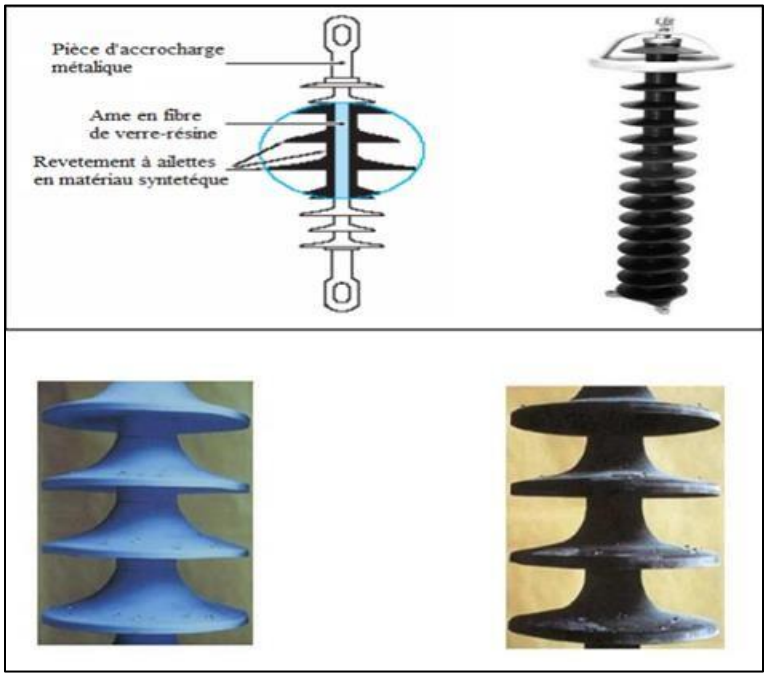

Figure I.2. *synthetic material insulators.*

I.4 Insulator Aging

Aging is primarily characterized by degradation of electrical, mechanical or chemical properties (for example, increased dielectric losses, decreased resistivity or loss of hydrophobicity). When subjected to various operational stresses, insulators age. Depending on the type of reaction produced on the composite material, several types of aging can be distinguished, the main ones being:

• Thermal aging caused by prolonged exposure to high temperatures on the dielectric.
• Electrochemical aging generated by certain processes whose origin is the electrolysis phenomenon occurring in the dielectric.
• Electrical aging (ionization - partial discharges) resulting from discharges on the surface and in cavities, especially gas pockets trapped within dielectrics. [18]

I.4.1 Thermal Aging

Thermal aging depends on the dielectric's structure. Material degradation is accelerated by the presence of oxygen. The main thermal aging processes are:
• Breaking of multimolecular chains, accompanied by degradation of electrical and mechanical properties,
• Release of low molecular weight gases,
• Oxidation leading to the formation of carboxylic acids. [18]

I.4.2 Electrochemical Aging

During the electrochemical aging process, the dielectric's temperature increases. This increase not only raises the material's conductivity but also activates the chemical reactions responsible for aging. [18]

I.5 Main Types of Insulators [19]:

I.5.1 Rigid-Type Insulators:

A rigid insulator (Figure II.3) is connected to the support by a fixed fitting. All standardized rigid insulators are delivered with an embedded socket, allowing them to be screwed directly onto

corresponding fittings. Ceramic and glass are the two materials used for rigid insulators. This type of insulator is used for overhead lines that do not exceed the voltage level of 60 kV.

Figure I.3 Cross-sectional view of a glass rigid insulator

I.5.2 Pin-and-Cap Insulators:

The pin-and-cap insulator (figure II.4) is composed of an insulating block bearing at its upper part a malleable cast iron sealed cap and internally a steel rod with grooves, whose conical head is also sealed in the glass or porcelain. The lower end of this rod is rounded and has the required dimensions to fit into the cap of the next element, and to be secured there by a cotter pin. The assembly consists of performing a sealing of the cap and the dielectric with cement, then that of the rod and the dielectric.

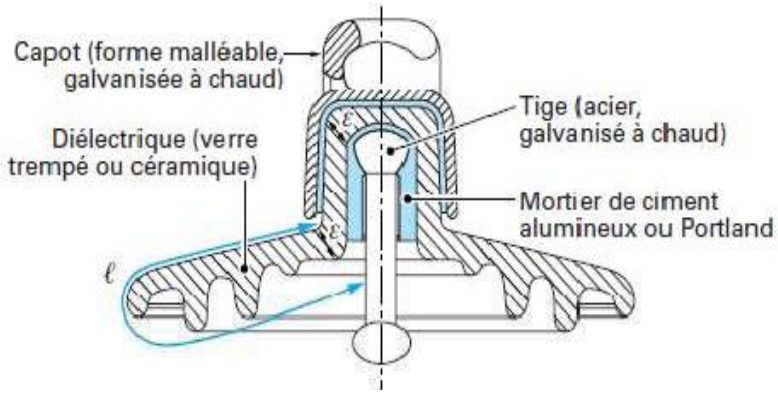

l : plus courte distance dans l'air, extérieure à l'isolateur e :longueur du canal de perforation, e << l / 2

Figure I.4: Pin-and-cap insulator

There exist multiple profiles of pin-and-cap insulators, designed for optimal performance according to the natural constraints of the site :

a- Standard profile:

The shape and dimensions comply with international standardization (IEC 305 1978), due to their flatness, well-spaced internal grooves, and creepage distance exceeding standard requirements. This type is widely used in medium-pollution areas.

Figure I.4.a: *Standard profile pin-and-cap insulator.*

b- Anti-fog profile (Type A):

Its diameter is larger than the standard profile. It features two or three deep grooves. The profile and wide groove spacing enable self-cleaning through wind and rain action. This design also facilitates easy manual washing when necessary.

Figure I.4.b: Anti-fog profile (Type A) pin-and-cap insulator

c- Anti-fog profile (Type B):

In this design, the thickness of the external groove acts as a barrier against fog and mineral salt deposits on the insulator surface, thereby preventing the formation of a conductive electrolyte layer.

This insulator type is effective in coastal areas.

Figure I.4.c: Fog-resistant profile (Type B) pin-and-cap insulator

d- Flat (Aerodynamic) profile:

The complete elimination of internal grooves reduces pollutant accumulation on the lower surface, thanks to air currents. This design is particularly effective in desert areas where rain-induced self-cleaning is infrequent.

This insulator type is predominantly used in the electrical regions of Touggourt, Hassi Messaoud, Ouargla, and El Oued.

Figure I.4.d: Flat (Aerodynamic) profile pin-and-cap insulator

e. Spherical Profile:

The spherical shape, with a large creepage distance and the absence of internal grooves, allows for easy and effective manual cleaning

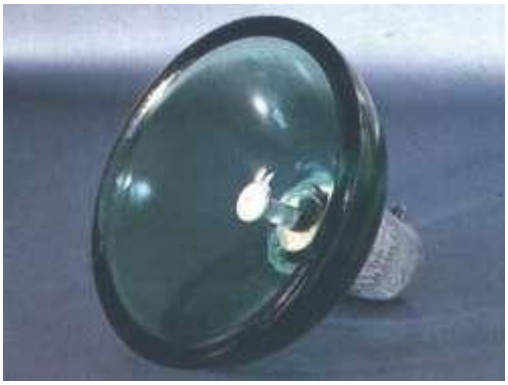

Figure I.4.e: *Spherical profile pin-and-cap insulator*

An insulator string (Figure II.5) consists of multiple pin-and-cap type elements or others. These elements are primarily subjected to tensile stresses. They are typically used in suspension applications and form insulator strings that are either:

- Vertical (alignement)
- Horizontal (anchoring)

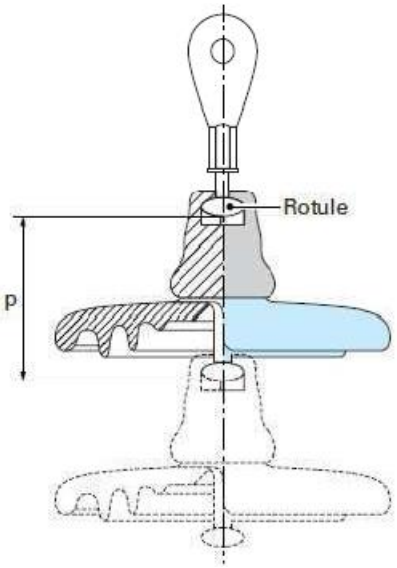

p: Nominal spacing

Figure I.5: Insulator string: clevis-and-ball assembly

I.5.3 Long-Rod Insulators:

This type can be either:

a) Composed of a solid ceramic or porcelain cylinder equipped with sheds (Fig II.6), with a metal connecting part at each end. This connection can be either an enveloping cap sealed around the conical ends of the cylinder or a rod-type fitting sealed into a designated cavity. Such insulators can be used individually or in series of several elements, depending on their length and the required insulation level.

b) Composed of a synthetic material, whose main characteristics are excellent pollution resistance, compact size, vandalism resistance, and light weight especially when compared to insulator strings used for high voltage power lines. This type of insulator is called a **composite insulator**, and it consists of three parts, each fulfilling a specific function:

A **fiberglass core**, impregnated with resin, capable of providing insulation and withstanding the mechanical stresses generated by the conductors.

A **hot-vulcanized EPDM (Ethylene Propylene Diene Monomer) elastomer housing**, which defines the profile and creepage distance while protecting the core against environmental aggressions. It also ensures sealing at the connection with the metal end-fittings. Its alternating shed profile enhances pollution performance.

Figure I.6: Long-rod insulators

I.6 Insulator Pollution

By definition, the term "pollution" refers to the degradation of a medium caused by the direct or indirect introduction of substances harmful to the environment or by the modification of its biological, chemical, or physical characteristics. This implies that when we talk about insulators, the phenomenon of pollution is defined as the degradation of the insulating surface by soluble electrolytes or non-soluble inert particles, which are substances capable of altering the electrical performance of the insulators [20].

The term "polluted," often associated with "dirty" in the usual sense, takes on another meaning when used to describe the condition of an insulator. In other words, a polluted insulator does not necessarily appear dirty. Indeed, an insulator that is heavily polluted by salt spray may appear clean while its electrical performance undergoes significant degradation. On the other hand, another insulator covered in soot, which appears dirty, may have remarkable electrical performance. Hence, an insulator is considered to increase the surface conductivity of that insulator. The term "contamination" is then more appropriate in this case to describe the phenomenon of insulator pollution, and it refers more to the electrical conductivity of the insulator surfaces than to their external appearance [20].

Even when well chosen, insulation is never immune to an incident. The severity of pollution at a site can change. The appearance of a new factory near a substation, the construction of a nearby road structure, or simply an exceptional weather event can increase, either permanently or temporarily, the pollution at a site where a substation or a line is already in operation. The initially correct sizing of the insulators may then become insufficient, and it is necessary to protect existing installations against new sources of pollution [21].

I.6.1 Types of Pollution

I.6.1.1 Natural Pollution

Natural pollution originates from [22]:

- Marine salts in coastal regions.
- Soil dust (especially during major construction projects).
- Sand carried by the wind in desert regions.

- **Marine Pollution**

In installations along the coast, spray carried by the wind gradually deposits a layer of salt on the insulators, which, over time, covers the entire surface of the insulator, including the best-protected parts. This salt layer, moistened by the spray itself, fog, or simply condensation, becomes conductive. Leakage current then flows through the surface layer, and electric arcs can occur under certain conditions, eventually leading to total flashover of the insulator [23].

- **Desert Pollution**

In desert regions, frequent sandstorms gradually deposit a layer of pollution containing salts on the surfaces of insulators . Once moistened, this layer becomes much more conductive and generates leakage current [21]. Which can abruptly lead to the appearance of partial arcs followed by total flashover of the insulator [22].

I.6.1.2 Industrial Pollution

This type of pollution is common in industrial areas, especially near factories and production facilities emitting smoke (refineries, cement plants, etc.). Additionally, exhaust gases from thermal power plants and fertilizers used in agriculture also contribute to deposits observed on the surface of insulators [24]]25].

In the presence of high humidity, the salt contained in these pollutants significantly reduces the surface resistivity of insulators, and flashover may occur [26].

Factories are not the only contributors to this kind of pollution; vehicle exhaust gases and fertilizers used in agriculture also contribute to the deposits observed on the surface of insulators [22].

I.6.1.3 Mixed Pollution

This type of pollution is actually the most common and severe for the operation of electrical facilities. Mixed pollution results from the combination of different types of pollution, such as marine and industrial pollution when industrial installations are located near the coast [22].

I.6.2 Classification of Pollution Types

The composition of this pollution varies depending on the sources of contamination and the conditions to which the insulators are subjected. The CES 815 standard provides a classification of pollution according to its origin. Essentially, the types of pollution that exist are natural pollution, industrial pollution, and mixed pollution [27].

Table I-1 Classification of Pollution According to Environmental Type:

Pollution Level	Examples of Typical Environments
I. Low	- Areas without industries and with low-density housing equipped with heating installations.
	- Areas with low density of industries or residences but often exposed to winds and/or rains.
	- Agricultural regions.
	- Mountainous regions.
II. Medium	- Areas with industries that do not produce particularly polluting fumes and/or with moderate density of housing equipped
	With heating installations.
	- Areas with high density of housing and/or industries but often exposed to winds and/or precipitation.
	- Areas exposed to sea winds, but not very close to the coast.
III. High	- Areas with high density of industries and suburbs of large cities with high density of polluting heating installations.
	- Areas located near the sea, or at least exposed to relatively strong winds coming from the sea.
IV. Very High	- Areas generally small in size, subject to conductive dust and industrial fumes producing particularly thick deposits.
	- Areas generally small in size, very close to the coast and exposed to strong winds and pollutants coming from the sea.

	- Desert areas characterized by long periods without rain, exposed to strong winds carrying sand and salt and subject to
	Regular condensation.

I.6.3 Insulator Behavior Under Polluted Conditions

The performance of insulators under polluted conditions is a critical factor in the design and operation of power lines in contaminated areas. Understanding the various conduction mechanisms under pollution is therefore essential.

When installing an insulator string, the total creepage distance is designed such that the electric field at any point remains well below the dielectric strength of the surrounding atmosphere. However, the surface conductivity introduced by pollution layers alters the voltage distribution along the leakage path, depending on the applied electrical stresses. Three distinct scenarios may occur:

1. Non-Stationary Arcing

- The electric arc extinguishes rapidly and re-ignites at different locations in succession.
- These intermittent arcs may result from:
    - **Dry band formation** caused by leakage current heating.
    - **Surface irregularities** (e.g., protrusions in the pollution layer).

2. Stationary Arcing

- The arc becomes fixed, either maintaining continuously (under DC) or re-igniting at the same spot (under AC).
- The combined impedance of the pollution deposit and the insulator surface limits the arc current and length.
    - If the current drops below a critical threshold, the arc self-extinguishes.
- **Thermal degradation** typically damages the insulator, necessitating replacement.

3. Pollution-Induced Flashover

Flashover in polluted insulators occurs due to the interaction of three key factors:

- **Deposition of conductive/semi-conductive pollutants**
- **Moisture absorption** (rain, fog, dew)
- **Applied voltage stress**

The flashover mechanism progresses through four distinct phases:

Phase 1: Leakage Current Initiation

- Conduction current flows through the electrolytic pollution layer, causing Joule heating.
- Increased temperature enhances electrolyte conductivity, creating a positive feedback loop.

Phase 2: Dry Band Formation

- Localized overheating evaporates moisture, creating high-resistance dry zones.

Phase 3: Partial Arcing

- Voltage concentrates across dry bands, initiating localized discharges.
- Arcing progressively expands the dry region.

Phase 4: Complete Flashover

- The arc bridges the electrodes along the insulator surface, causing full breakdown.

The progression through these phases depends on multiple parameters:

- **System voltage**
- **Pollution layer conductivity**
- **Dry band width**
- **Insulator profile geometry**
- **Total creepage distance**

I.7 Conclusion :

Insulators account for a very modest percentage of the cost of a medium-voltage overhead line. However, they are essential components on which the operational safety, quality, and continuity of service depend.

Before carrying out any high-voltage project, a study to determine the pollution level of the concerned site must necessarily be conducted. This is essential to ensure proper insulation design and selection. Indeed, it is recommended that this pollution level study be based on experimentation conducted over the longest possible period, because the severity of a site's pollution can change. The appearance of a new factory near a substation or line, the construction of a nearby road, or even an exceptional weather event can increase, either temporarily or permanently, the pollution at the site—while a substation or line is already in operation there.

What was initially a correctly designed insulation system may then become inadequate, and existing installations must be protected against potential new sources of pollution.

CHAPTER II

OPTIMIZING HIGH VOLTAGE INSULATOR SURFACE DESIGN USING TEXTURED POLYMERIC INSULATORS

Chapter II: Optimizing High Voltage Insulator Surface Design Using Textured Polymeric Insulators

II.1 Introduction:

High-voltage insulators are critical components in electrical power systems, ensuring safe and efficient transmission by preventing unwanted current leakage. However, environmental factors such as pollution, moisture, and surface contamination can lead to flashovers, compromising insulation performance and grid reliability. To address these challenges, researchers have explored advanced materials and surface engineering techniques, with textured polymeric insulators emerging as a promising solution.

Polymeric insulators, known for their lightweight, hydrophobic properties and resistance to vandalism, offer advantages over traditional ceramic and glass insulators. By introducing controlled surface textures—such as micro- or Nano-patterns—engineers can further enhance their performance. These textures can :

- **Improve hydrophobicity**, reducing water film formation and minimizing leakage currents.
- **Mitigate pollution accumulation**, by creating self-cleaning effects through reduced adhesion of contaminants.
- **Enhance flashover resistance**, by disrupting conductive paths along the insulator surface.

This study focuses on optimizing the surface design of polymeric insulators through texturing techniques, evaluating their electrical performance under various environmental conditions. By leveraging computational modeling, material characterization, and high-voltage testing, we aim to identify the most effective surface patterns for maximizing insulation reliability in real-world applications.

The findings could lead to the development of next-generation insulators with extended service life, reduced maintenance costs, and improved resilience in harsh operating environments.

II.2 Texturing of polymeric insulators

The extensive use of polymeric materials, and especially hydrophobicity transfer materials like silicone rubber for composite insulators, did not lead to the total elimination of pollution flashover. Severe ambient conditions would still result in partial discharging on the insulator surface and the design of polymeric insulators remains very simple mainly due to the moulding restrictions inhibiting the development of re-entrant profiles [28].

The surface leakage current on a polluted polymeric insulator has the highest density in the regions of the smallest contour perimeter which are the shank sections. Consequently, the surface electric field strength is also at its highest at these regions resulting in increased surface power dissipation. Heating is proportional to the power dissipation. Therefore, local heating leads to the formation of dry-bands and the damaging effect induced by the associated surface discharges.

Textured insulators are a novel approach [29] for the design of polymeric insulators that takes advantage of the moulding properties of silicone rubber. Fine texturing of the polymeric surface could be achieved by employing a pattern consisting of an array of contiguous or overlapping protuberances. The aim of this design is to reduce the surface power dissipation by reducing both the electric field and current density, This could be achieved by increasing both the surface area and the creepage distance of the insulator without increasing the overall longitudinal length of the insulator [28]. Moreover, textured patterns were expected to alleviate the damage induced on polymeric materials due to surface discharges, compared with non-textured samples of the same material, by introducing multiple paths for current conduction: as soon as one current path starts to dry as a result of Joule heating, its resistance will increase. However, the current flow will switch to an alternative path of lower resistance before severe thermal damage occurs [28].

II.2.1 Surface patterns

The geometry of such protuberances could be hyperboloidal, conical and pyramidal or other symmetrical shapes each resulting in a different variation of the surface area [28].

Figure II.1 shows a side view of a protuberance that is formed as part of a sphere and has a height, c, and a base as a circle of radius, a. The radius of the sphere is b. Also, the top view of an array of contiguous part-spherical protuberances is shown (Figure II.1b).

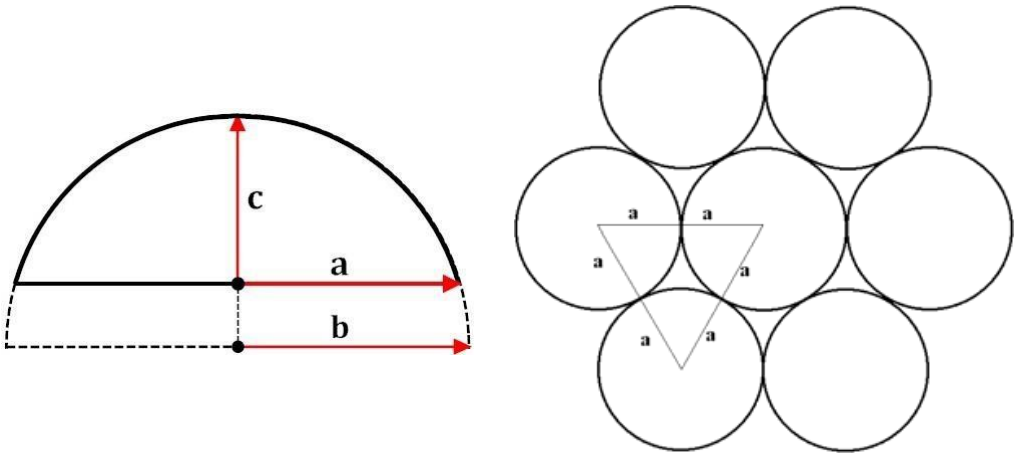

(a) (b)

Figure II-1. Side view of part-spherical protuberance (a) and top view of an array of contiguous part-spherical protuberances (b) [29].

Therefore, we can write

$$a^2 = c(2b - c) \quad \textbf{(1)}$$

And the surface area of the spherical cap will be

$$A_p = 2\pi bc \quad \textbf{(2)}$$

From Figure 1-b, the area of the triangular plane surface is

$$A_t = \sqrt{3}\mathrm{a}^2 \quad \textbf{(3)}$$

The three neighboring protuberance will increase this surface area to

$$A_{pt} = \frac{A_p}{2} + A_t - \frac{\pi \mathrm{a}^2}{2} \quad \textbf{(4)}$$

$$A_{pt} = \mathrm{a}^2 \left[\frac{\pi b}{2\ \mathrm{b-c}} + \sqrt{3} - \frac{\pi}{2}\right] \quad \textbf{(5)}$$

Therefore, the spherical protuberances will increase the surface area by a ratio

$$\frac{A_{pt}}{A_t} = 1 + \frac{\pi c}{2\sqrt{3}(2b-c)} \quad \textbf{(6)}$$

Equation (2-23) is suggesting that, for protuberances that are formed as part of spheres, the increase of the surface area is dependent on the height of the sphere cap and on the radius of the sphere. If the protuberance is a hemisphere ($b = c$) then the ratio for a contiguous hemispherical pattern will be

$$\left.\frac{A_{pt}}{A_t}\right|_{b=c} = 1 + \frac{\pi}{2\sqrt{3}} = 1.907 \quad \textbf{(7)}$$

which is independent of the hemisphere radius b. For a tightly arranged array of adjacent hemispherical protuberances, the surface will increase close to a limiting value of 2, which is the ratio of the hemisphere surface to the surface of the circular base. Ratios greater than 2 can be achieved by utilising other geometrical arrangements [2].

The typical approach for the design of outdoor insulators for polluted environments is the increase of the creepage distance per unit of axial length. The textured patterns aim to achieve both longer creepage and an increase of the surface area. For hemispherical protuberances, other patterns have been explored where the protuberances are overlapping forming intersections. Figure II.2. shows such geometrical configurations along with the contiguous pattern (Figure II.2. A). The arrows indicate the circular arc paths formed by the intersections. Pattern B follows a hexagonal intersection of overlapping hemispherical protuberances while the intersections of patterns C and D have a square and triangular shape respectively [28].

Returning to the example of the contiguous hemispherical protuberances pattern (Figure II.2. A), the creepage distance per row in the direction of the electric field is 2.093a while the distance on the plane surface is √3a, marking an per unit increase of the creepage distance by a factor of 1.209, resulting in a substantial decrease of both *E* and *J* [28]. The creepage factor is also independent of the hemisphere radius.

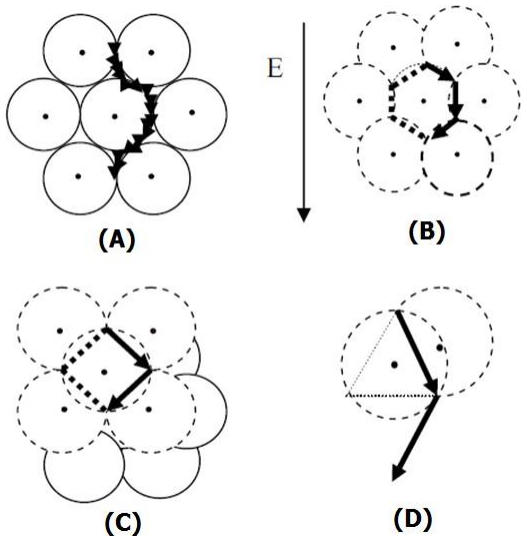

Figure II.2. Textured patterns: contiguous hexagonal (A), intersecting hexagonal (B), intersecting square (C) and intersecting triangular (D) [29].

II.2.2 Power dissipation factor

Assuming that the plain and textured surfaces are covered by a pollution layer of same thickness t (metres) and conductivity σ (Siemens/metre), then the layer conductance is $k = t \cdot \sigma$ (Siemens) and is the same for both surfaces. For an insulator leakage current I, at position where the insulator circumference is C (metres) the current density inside the pollution layer is $J_{layer} = I/Ct$ (A·m^{-2}). As the thickness of layer t is constant, this can be expressed as a surface current density $J = J_{layer} \cdot t$ (A·m^{-1}).

For a given insulator region, if the surface area is increased by a factor α, consequently the current density J will be reduced by the same factor (Jplain/Jtextured = α). Similarly, if a textured pattern increases the creepage distance by a factor β, the electric field strength will be reduced by the same factor as well (Eplain/Etextured = β) Given that power dissipation is related with E and J according to the relationship given by Equation (2-2), a textured pattern would reduce the surface power dissipation per unit area of the insulator surface P (W·m^{-2}) by a combined factor $\alpha \times \beta$:

$$\frac{P_{\text{plain}}}{P_{\text{textured}}} = \frac{E_{\text{plain}} \cdot J_{\text{plain}}}{E_{\text{textured}} \cdot J_{\text{textured}}} = \alpha \times \beta \qquad \textbf{(8)}$$

While the well-established anti-fog designs increase only the creepage distance, thus affecting only factor β, textured patterns could control both the surface area (factor α) and the

creepage distance (factor β) independently, thus achieving different combined power density factors $\alpha \times \beta$. This combined factor could function as a figure of merit for the ability of the textured design to inhibit the drying of the pollution layer by decreasing the surface power dissipation.

II.2.3 Theoretical classification of candidate textures

A theoretical classification of the candidate textures that would be assessed for the development of textured insulator prototypes was conducted based of the combined power density factor. Geometrical calculations on the patterns shown in Figure II.2 are shown in Table II-1.

Table II-1. Theoretical classification of textured patterns. Table adopted from [28].

Texture	Area factor α	Creepage factor β	Power density factor αβ
1. Contiguous hexagonal	1.907	1.209	2.306
2. Intersecting hexagonal	1.446	2.356	3.407
3. Intersecting square	1.301	2.222	2.891
4. Intersecting triangular	1.209	1.814	2.193

The calculations presented in the above table suggested that based on the power density factor as a figure of merit for the anti-dry band performance, the contiguous hexagonal, the intersecting hexagonal and the intersecting square patterns were the most promising textures.

Early-stage tests reported in [28] on non-textured silicone rubber samples and silicone rubber samples with a textured finish, similar to the contiguous configuration, showed some promising results. The present research work will describe the laboratory investigations of these textured patterns in a series of material tests and the development and testing of full textured insulators in clean-fog tests.

II.3 INSULATOR PROFILE AND TEXTURES [30]

II.3.1 CONVENTIONAL INSULATOR PROFILE

The conventional (CONV) insulator geometry used here, for which clean-fog pollution test results have already been reported **[31]** , has a surface creepage distance of 375 mm and a form

factor of 2.76. The textured insulator prototypes use the same basic profile, but with the texture moulded either on the insulator trunk alone (TT profile) or on both the trunk and the shed undersides (TTS profile).

II.3.2 TEXTURED-TRUNK (TT) INSULATORS

For these insulators, the three trunk sections have been moulded with a square-intersection, hemispherical protuberance 4 mm (TT4) or 6 mm (TT6) diameter cylindrical

pattern based on the plane sample of Figure 1, where all intersections are again aligned at a

45-degree angle to the axial voltage gradient. The insulator sheds were not textured. A TT4

insulator CAD image is shown in Figure 3. The surface creepage distance is increased by this texture to approximately 471 mm (Table II.2).

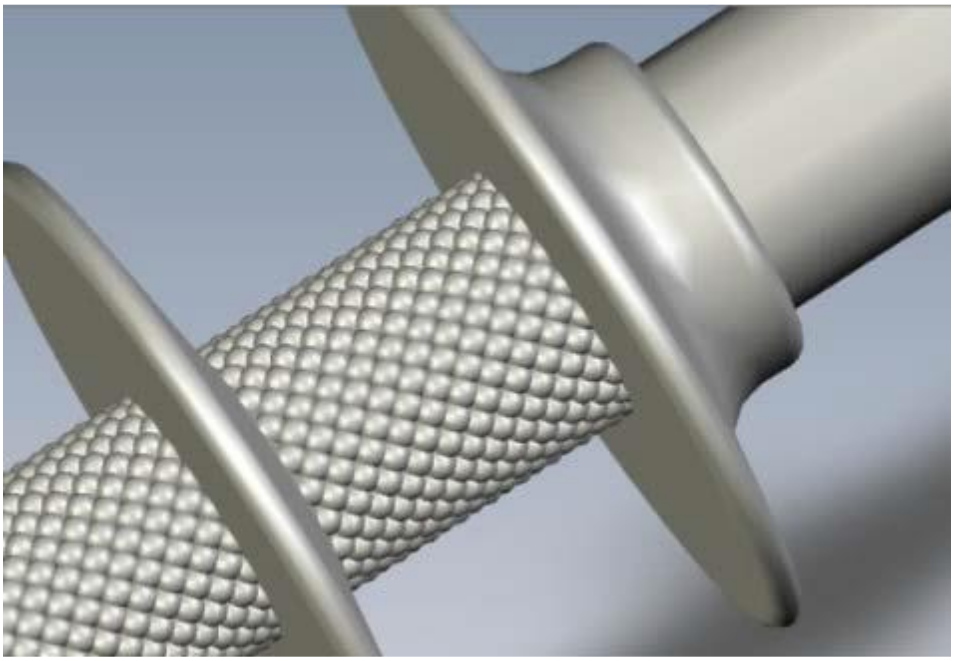

Figure II.3 *4mm textured trunk insulator (TT4). CAD image.*

II.3.2.1 CREEPAGE DISTANCE OF TEXTURED TRUNK

Figure 4 is a plan representation of a region of square intersection hemispheres of radius a. A creepage factor β will describe the per-unit increase of surface length in the direction

of voltage gradient compared with a non-textured surface. For a moist pollution layer, current flow is found (from infrared imaging) to be significant along the intersections at 45° to the axis

where evaporation is less effective. For paths along intersections, e.g. *abc*, which are formed by two semicircles of radius a/√2, $\beta = \pi / \sqrt{2} = 2.22$ (1)

This has important implications for the reduction of insulator leakage current by texturing when a moist conducting pollution layer lies on the surface, especially if loss of hydrophobicity is present.

II.3.2.2 TEXTURED TRUNK AND SHED INSULATORS (TTS)

II.3.2.2.1 UNDERSHED TEXTURE DESIGN

In this case, the intersecting-square textured trunks were accompanied by insulator shed undersides with suitable texturing to obtain 45° orientation and a further increase of the creepage distance. This was achieved with a logarithmic (Bernoulli) double spiral pattern of semi-cylindrical ridges

(Figure 5) which presents a series of semi-elliptical paths to the radial leakage current, and increases the shed underside creepage distance by a per-unit factor of $\beta = 1.35$. The overall creepage distance for the TTS design is 503 mm. This distance is independent of the hemisphere and ridge radii (Table 1).

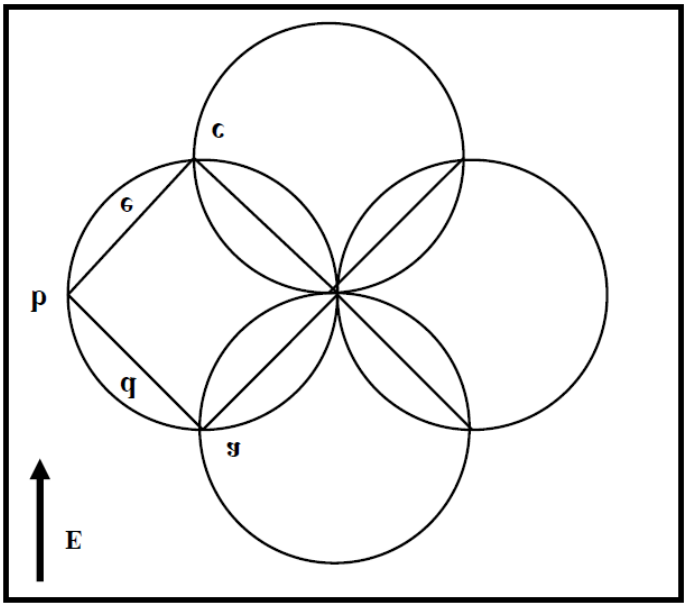

Figure II.4. *Hemispherical protuberances: square-intersection geometry.*

Table 1. Creepage distances for conventional and textured insulators.

Insulator design	Maximum creepage distance (mm)
Conventional (CONV)	375
Textured trunk 4mm (TT4)	471
Textured trunk & shed 4mm (TTS4)	503
Textured trunk 6mm (TT6)	471
Textured trunk & shed 6mm (TTS6)	503

Table II.2 Creepage distances for conventional and textured insulators.

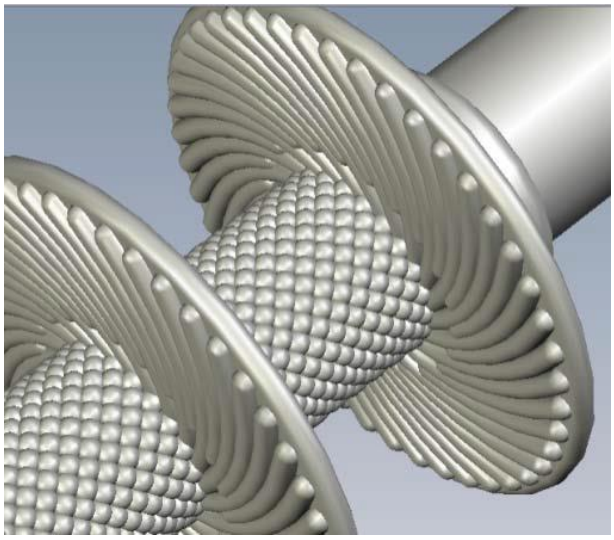

Figure II.5. *TTS6 insulator: detail of the double ridge pattern of the shed underside and the junction with the shank texture (CAD image).*

II.3.2.2.2 Creepage distance of textured shed

The pattern of semi-circular cross-section ridges with their tangent maintained at a constant 45° to the radius is described for the *n* th ridge by the polar-coordinate equation

$$r / r_0 = \exp[\theta] = \exp[\gamma + n\delta] \qquad \textbf{(9)}$$

The angular interval δ (see Figure 6) between successive ridges is chosen to provide alignment and continuity with the texture of the square-pattern shank, at the junction between the shank and the shed underside. The semi-circular diameter of each ridge was 4mm for TTS4 profiles and 6mm for TTS6 profiles. The inner and outer spiral radii *r0* and *r* were chosen to match the radial shank and shed dimensions (14 mm and 45 mm) of the insulator. The inner end of each spiral replaced the

top row of the protuberance on the shank; the outer end was spherically profiled. A closer ridge pattern over the shed underside could be achieved by a nested pair of spiral structures. The textured trunk and shed design which employed this double-ridge pattern is also shown in Figure 5.

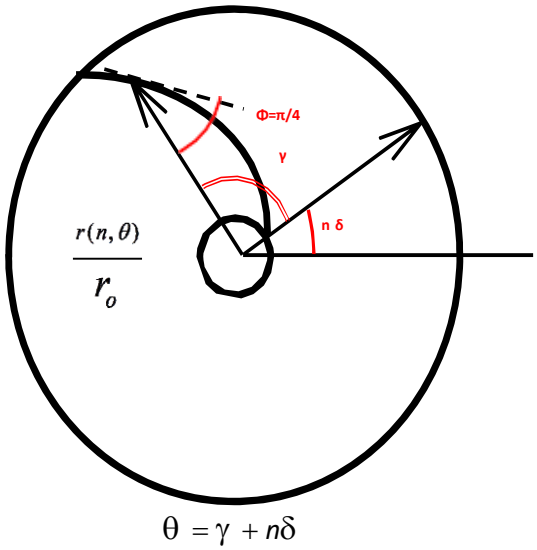

Figure II. 6. *Logarithmic spiral of constant angle 45°.*

II.3.2.3 ARTIFICIAL POLLUTION OF INSULATORS FOR CLEAN-FOG TESTS

Sodium chloride was added to a suspension of 40 g/l of kaolin and 1 g/l of Triton X-100 wetting agent to obtain volume conductivities of 4 S/m (for 27 g/l NaCl), 8 S/m (65 g/l NaCl),

11.2 S/m (100 g/l NaCl) or 20 S/m (260 g/l NaCl). Conventional and textured insulators wetted with this suspension were dried for 24 hours and tested usually within 48 hours. The values of mean salt deposit density (SDD) resulting from these suspensions were measured using standard procedures [32] to be 0.21 mg/cm2, 0.42 mg/cm2, 0.64 mg/cm2 or 1.15 mg/cm2. The kaolin non-soluble deposit

density (NSDD) was about 0.1 mg/cm2. Importantly, the mean SDD values for the textured surfaces were found to be not significantly different from those for plain surfaces.

II.4 COMPARATIVE CLEAN-FOG TESTS

II.4.1 TEST PROCEDURES

The 150 kVA, 50 Hz, 50 kV, 2 A transformer was programmed to deliver a ramp voltage at 4 kV/minute until flashover occurred. Voltage and current were both recorded with 16-bit data acquisition at a sampling rate of 104 per second. A LabView program was used to file, display, process and post-process these data.

II.4.2 MEAN FLASHOVER VOLTAGES (FOV)

In clean-fog chamber tests, the choice of water supply rate to the spray nozzles (and thus the fog density) to control the insulator wetting rate is important. For conventional insulators, the flashover voltage is to be reduced to a minimum value for a ramp voltage applied at the commencement of fog generation with a spray rate of 8 l/h [**31**].

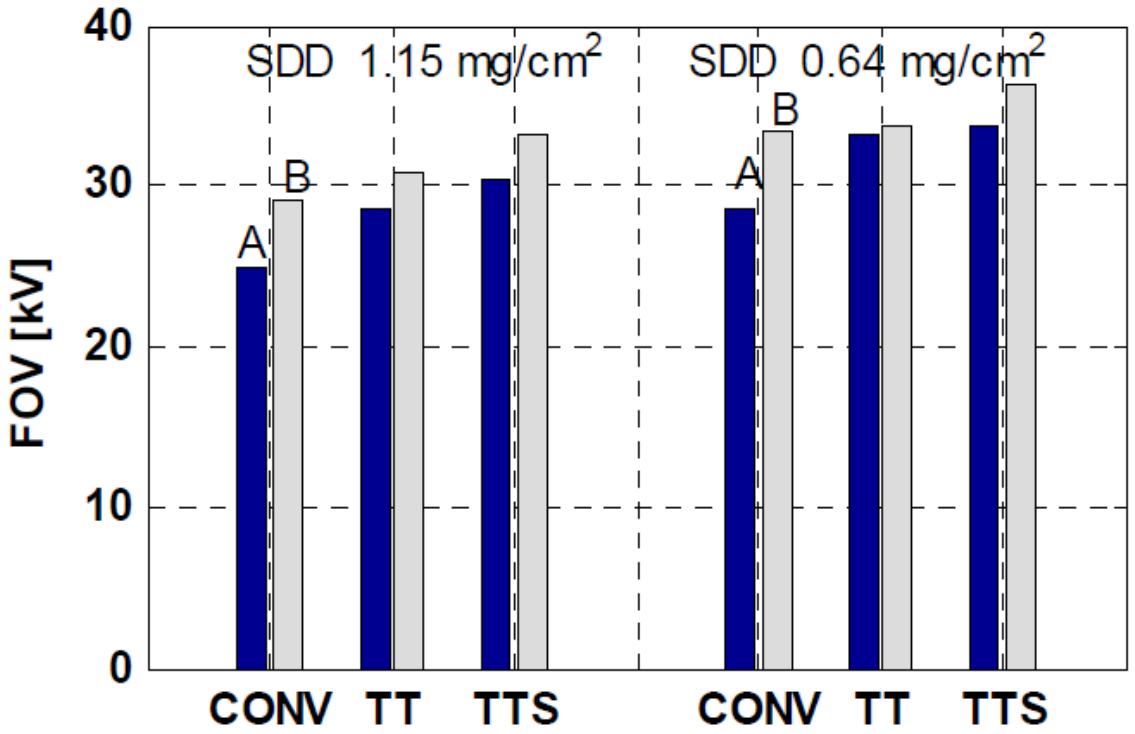

Figure II. 7. *Mean FOV for textured and conventional insulators. Material A and B (dark and light grey respectively) Fog spray rate 3 l/hr. Two SDD levels.*

A spray rate of 3 l/h, on the other hand, produces a Ushaped characteristic where the minimum flashover voltage occurs on the second or third ramp. These same two spray rates have been used here for textured insulators so that direct comparison can be made. Every polluted insulator was subjected to a number of series of flashovers, each series consisting between 4 and 9 ramp voltages.

The flashover voltages listed in Table II.3 for each series are all calculated as the mean value from the first four flashovers.

Table II.3. Test results (include only the first 4 ramps of each series).

Test conditions		Material	Insulator	Number of test series	Number of flashovers	Mean FOV [kV]
Pollution level (SDD)	Fog rate (l/h)					
Severe pollution (1.15 mg/cm^2)	lower flow rate (3 l/h)	A	CONVA	2	8	24.9
			TT4A	1	4	28.6
			TTS4A	2	8	30.4
		B	CONVB	1	4	29.0
			TT6B	1	4	30.9
			TTS6B	3	12	33.2
	higher flow rate (8 l/h)	A	CONVA	4	16	22.8
		B	CONVB	4	16	23.4
			TT6B	2	8	24.0
High pollution (0.64 mg/cm^2)	lower flow rate (3 l/h)	A	CONVA	6	24	28.6
			TT4A	7	28	33.2
			TTS4A	7	28	33.8
		B	CONVB	5	20	33.3
			TT6B	7	28	33.8
			TTS6B	6	24	36.2
	higher flow rate (8 l/h)	A	CONVA	5	20	28.3
			TT4A	6	24	34.3
			TTS4A	6	24	35.6
Moderate pollution (0.42 mg/cm^2)	lower flow rate (3 l/h)	A	CONVA	2	8	30.1
		B	CONVB	1	4	36.3
			TT6B	1	4	40.5
			TTS6B	1	4	38.9
	higher flow rate (8 l/h)	A	CONVA	2	8	31.2
		B	CONVB	3	12	33.9
			TT6B	7	28	34.7
			TTS6B	1	4	34.5
Lower pollution (0.21 mg/cm^2)	higher flow rate (8 l/h)	A	CONVA	1	4	41.2
			TT4A	1	4	44.9

II.4.3 COMPARISON OF FOV FOR TEXTURED AND CONVENTIONAL INSULATORS

As an example of comparative performance of the different materials A and B, it is useful to examine flashover voltages for insulators polluted with SDD levels of 0.64 and 1.15 mg/cm2 (Figure 7). Important conclusions can be drawn:

• Insulator texture improves the FOV by up to 27% for material A and by up to 10% for material B;

• The superior FOV of insulators of material B are nearly matched by those of material A, if the insulators are textured.

II.4.4 FOV VARIATION WITH DEGREE OF POLLUTION

Figures 8a and 8b, for insulators of materials A and B respectively, confirm that the test procedure is able to reveal the fall of mean FOV with increasing pollution level for all series of ramps and both spray rates. They also demonstrate that the improvement in FOV of the textured insulators is greater at the higher pollution levels, and so effectively raises the lowest FOV for both materials.

II.4.5 FOV VARIATION DURING RAMP TEST SERIES

An example is shown in Figure 9 of FOV variation in a set of six long (8-ramp) series for the TTS4A insulator.

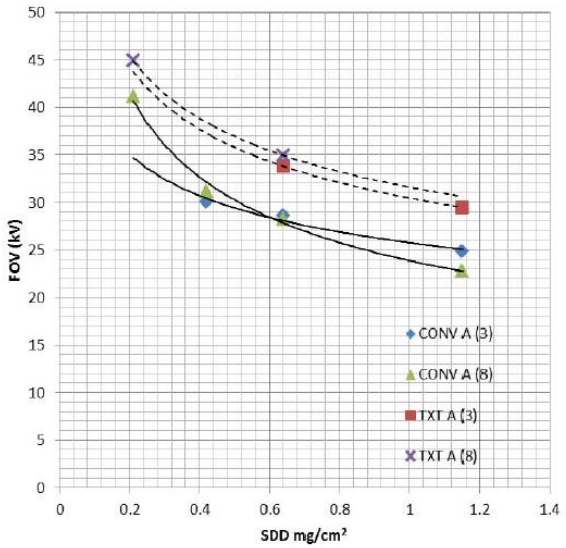

Figure II.8a. *FOV reduction with increasing SDD (material A) Fog spray rates 3 and 8 l/h. TXT values are mean of TT and TTS FOVs*

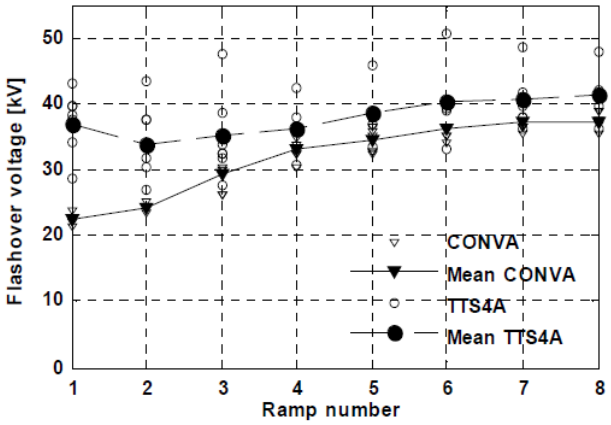

Figure II. 9. *Mean FOV of 6 test series for TTS4 silicone rubber insulators. Material A. Each series consists of 8 ramp voltage tests. SDD 0.64 mg/cm2. Fog spray rate 8 l/h.*

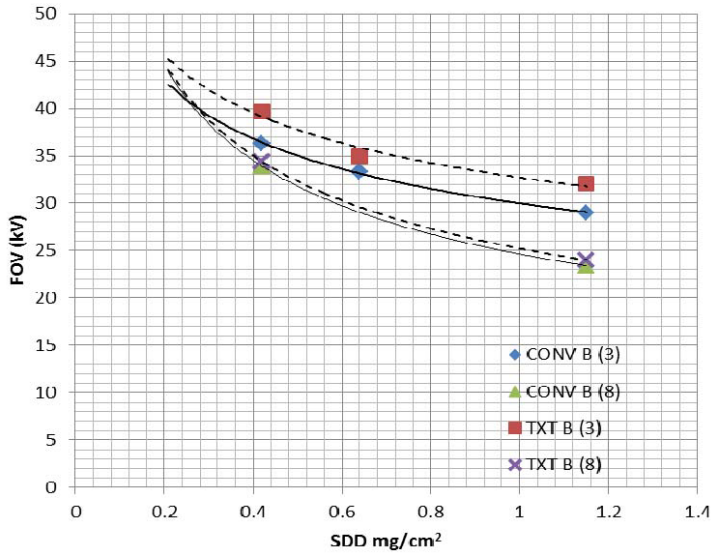

Figure II. 8b. *FOV reduction with increasing SDD (material B) Fog spray rates 3 and 8 l/h. TXT values are mean of TT and TTS FOVs.*

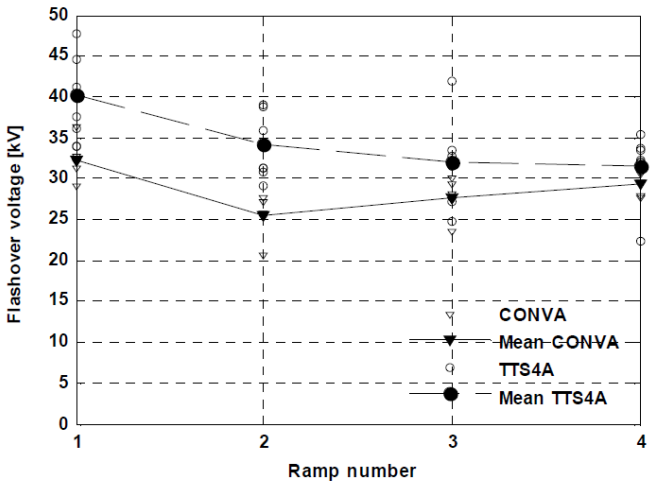

Figure II.10. *Mean FOV of 6 test series for TTS4 silicone rubber insulators. Material A. Each series consists of 4 ramp voltage tests. SDD 0.64mg/cm2. Fog spray rate 3l/h.*

Measurements for the CONV A insulator are also shown, which at this higher spray rate invariably shows the minimum FOV to occur for the first ramp voltage application of every series. The textured insulator, in contrast, shows a less severe reduction, and the minimum FOV occurs for the second ramp voltage. Since each individual ramp test in a series is up to 10 minutes in duration before flashover, with a 5-minutes interval between ramps, this indicates a much slower fall in insulator strength for the textured insulator. The same comparison is shown in Figure 10 for the lower spray rate, where both conventional and textured insulators show a U-shape FOV characteristic during the ramp series. The fall is again slower for the textured insulator.

II.5 LEAKAGE CURRENT AND DATA PROCESSING

II.5.1 TIME WINDOWS

The data acquisition system enabled current and voltage both to be sampled and stored at a rate of 200 samples per second throughout each ramp test. r.m.s. values of leakage current and ramp voltage were computed both for successive cycles (20 ms windows) and over sets of 100 cycles (2 s windows). The longer window enabled trend analysis of preflashover events.

II.5.2 20 ms (SINGLE-CYCLE) WINDOW

Figure 11a shows the FOV variation during an 8-ramp series with the TT4 insulator (material A), and Figures 11b, 11c, 11d are examples of r.m.s. voltage and current for selected ramps 1, 3 and 8 of this series. Also shown is the associated leakage resistance calculated from the ratio of mean power and mean square current.

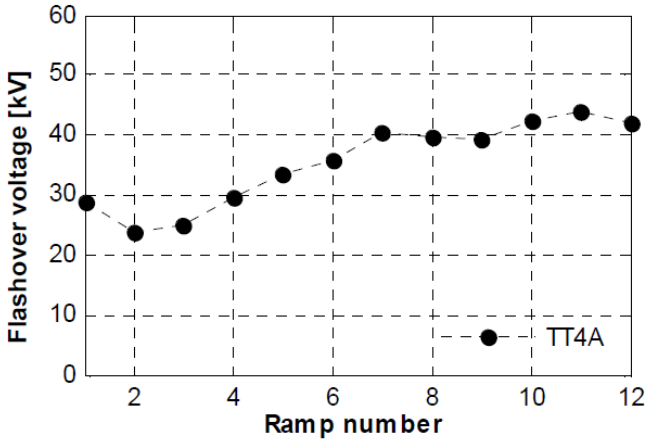

Figure II.11a. *Ramp voltage test series for TT4A insulator under conditions of high pollution (0.64 mg/cm2) and higher fog spray rate (8 l/h).*

These electrical data provide a valuable insight to the FOV behaviour in several respects:

a) At 28.9 kV, the FOV of the TT4A insulator (insulator TT4 with material A) for ramp 1 is significantly higher than the initial 21.6 kV FOV which was found for the conventional insulator (CONVA) in the tests of Part 1, and it is correspondingly found here that the leakage current measurement for TT4A is much lower (3mA at 25 kV) than was the case for CONVA (20 mA at 20 kV). This illustrates the inverse relationship of the leakage current with the subsequent FOV.

b) For TT4A), the U-characteristic of FOV in Figure 11a is again accompanied by an inverse variation of the preflashover current, which for ramps 1, 3 and 8 at 25 kV is respectively 3, 50 and 7 mA.

c) For both insulator types and all ramps, the immediate pre-flashover parameters of power loss and energy dissipation per cycle are all in the range 500-1000 W and 10-20 Joules.

II.5.3 2 s (100-CYCLE) WINDOW

Figure 12 displays data in terms of the time before flashover (TBF) which facilitates comparison between ramp tests of different time duration by using the common event of insulator flashover.

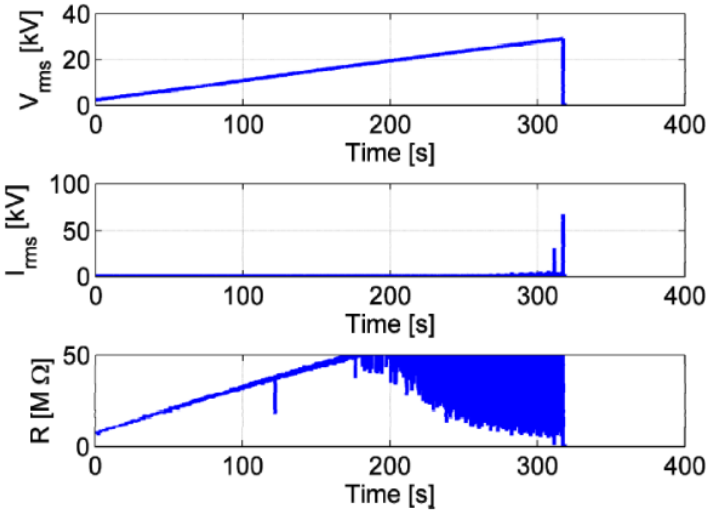

Figure II.11b. *Ramp 1 of test series for TT4A insulator under conditions of high pollution (0.64 mg/cm2) and higher fog spray rate (8 l/h). FOV 28.9 kV at 320 s.*

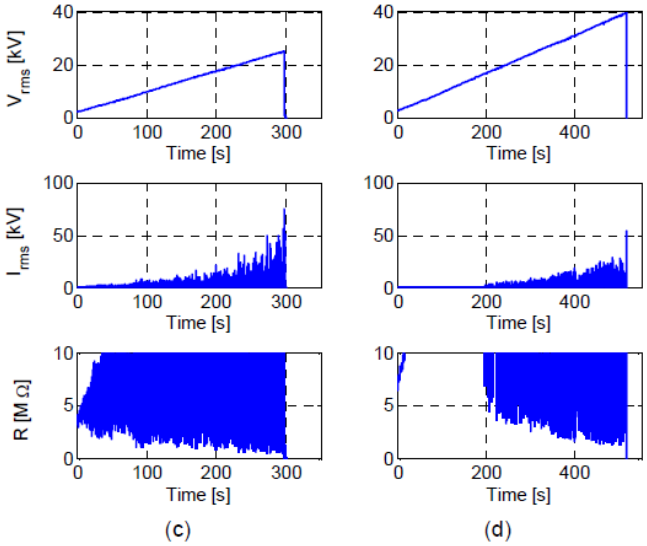

Figure II.11 c,d. *Ramps 3 and 8 of test series for TT4A insulator under conditions of high pollution (0.64 mg/cm2) and higher fog spray rate (8 l/h). Ramp3: FOV 25.2 kV at 301 s; Ramp8: FOV 39.7 kV at 520 s.*

In addition to the test voltage, current and the mean power dissipation P, derived data associated with the level of discharge activity can be obtained using the longer window. For example, the number N of discharges per second (peaks greater than 0.5 mA) allows the ratios Irms/N and Pav/N to be calculated. Then, the ratio Q = Irms/N (coulombs) represents the rms average of charge flow per discharge during each 2s window and the ratio W = Pav/N (joules) quantifies the corresponding mean energy loss per discharge. Figures 12a, 12b and 12c, 12d show, for TT and TTS textured insulators of materials A and B respectively under conditions of higher pollution (0.64 mg/cm2) and lower fog spray rate (3 l/h), the 2 s r.m.s. voltage, current and derived

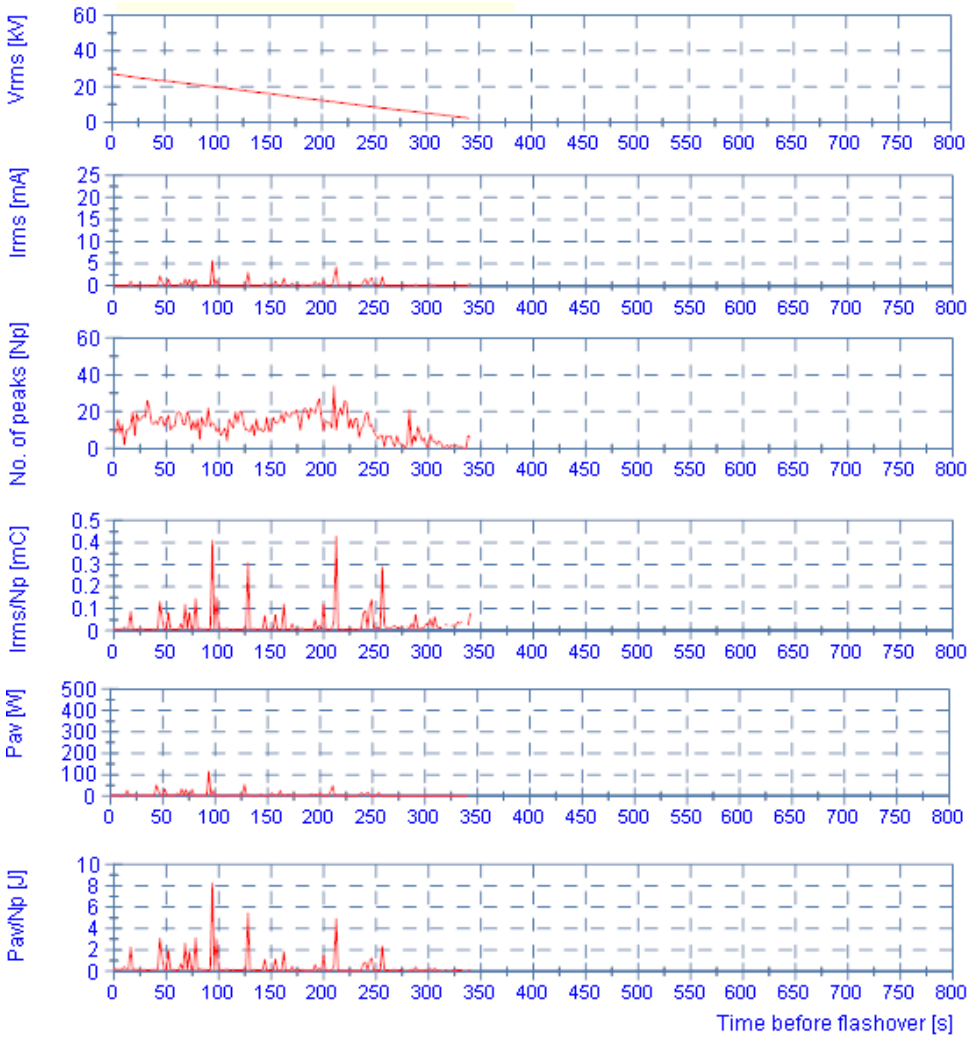

Figure II.12a. *Analysis (2 s window) of ramp voltage data for a TT4 insulator, for high pollution (0.64mg/cm2) and lower fog spray rate (3l/h) (3rd ramp). FOV 27 kV at 340 s.*

data for different ramp series These can be compared with similar records in Part 1 of this paper obtained in the same test conditions for conventional non-textured insulators, when it becomes clear that:

• The pre-flashover current is significantly lower for textured insulators;

• For conventional insulators, the pre-flashover discharge activity N is found to decrease as

flashover is approached, accompanied by large current transients. This trend is usually absent for textured insulators;

• For material A, the charge flow Q and energy dissipation, W, are an order of magnitude smaller for the textured insulators. For material B, these parameters are comparable for both conventional and textured insulators. A further comparison of the textured and conventional designs can be obtained from a computation of leakage resistance. As the test voltage ramp increases towards the FOV, the variation of leakage resistance $R = P_{av}/I^2$ rms represents the combined resistance of the decreasing unbridged sections of the pollution layer in series with the growing discharge channels. Figure 13 shows examples of the transient variations of R for a conventional insulator with FOV = 27.5 kV and a TTS4 insulator of FOV = 35.5 kV both fabricated with material A. Both show a trend of a decrease in R with increasing voltage, but it is clear that the higher FOV of the textured insulator is associated with its higher leakage resistance throughout the test.

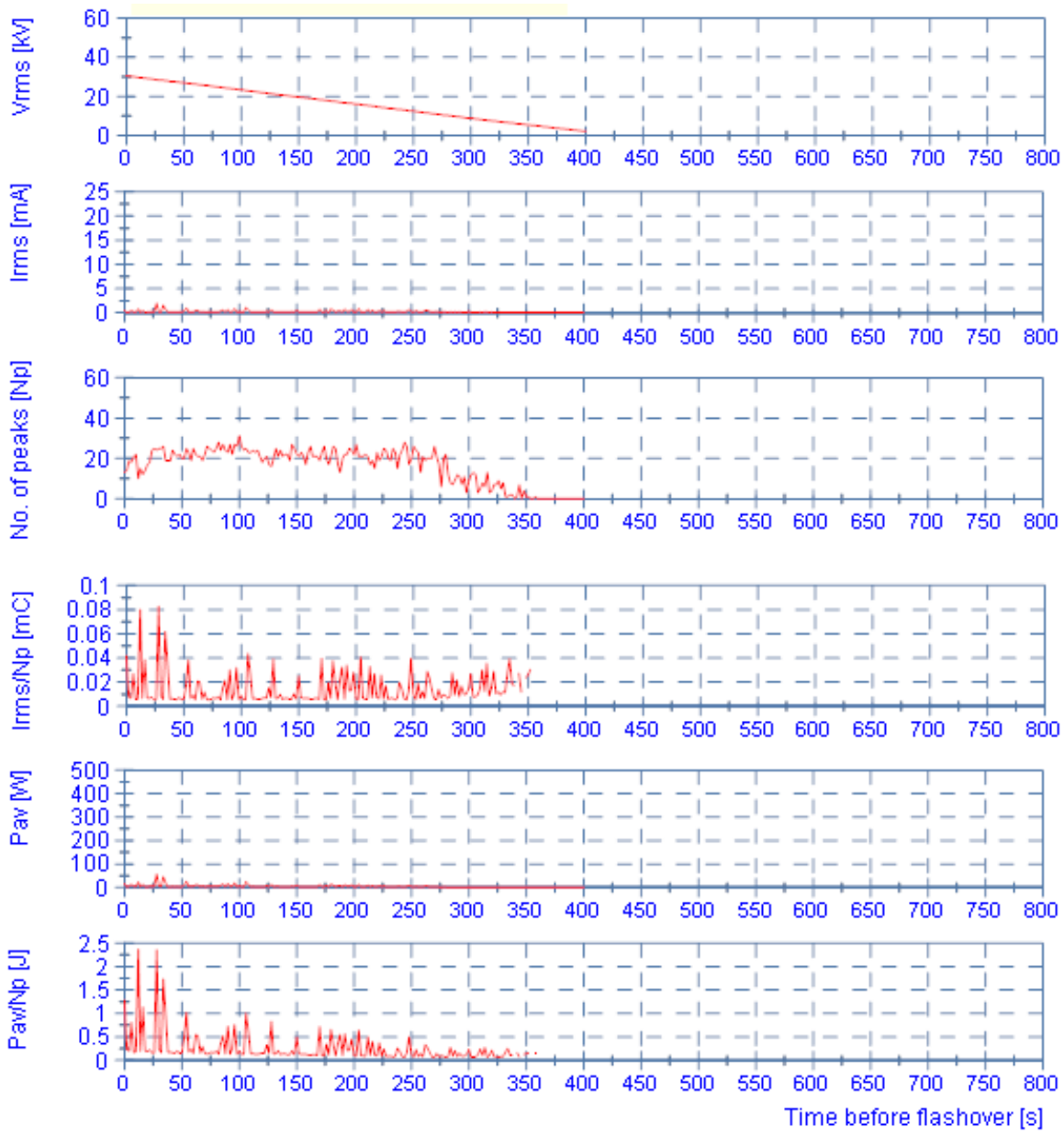

Figure II.12b. *Analysis (2 s window) of ramp voltage data for a TTS4A insulator, for high pollution (0.64 mg/cm2) and lower fog spray rate (3l/h) (3rd ramp). FOV 30.6 kV at 400 s.*

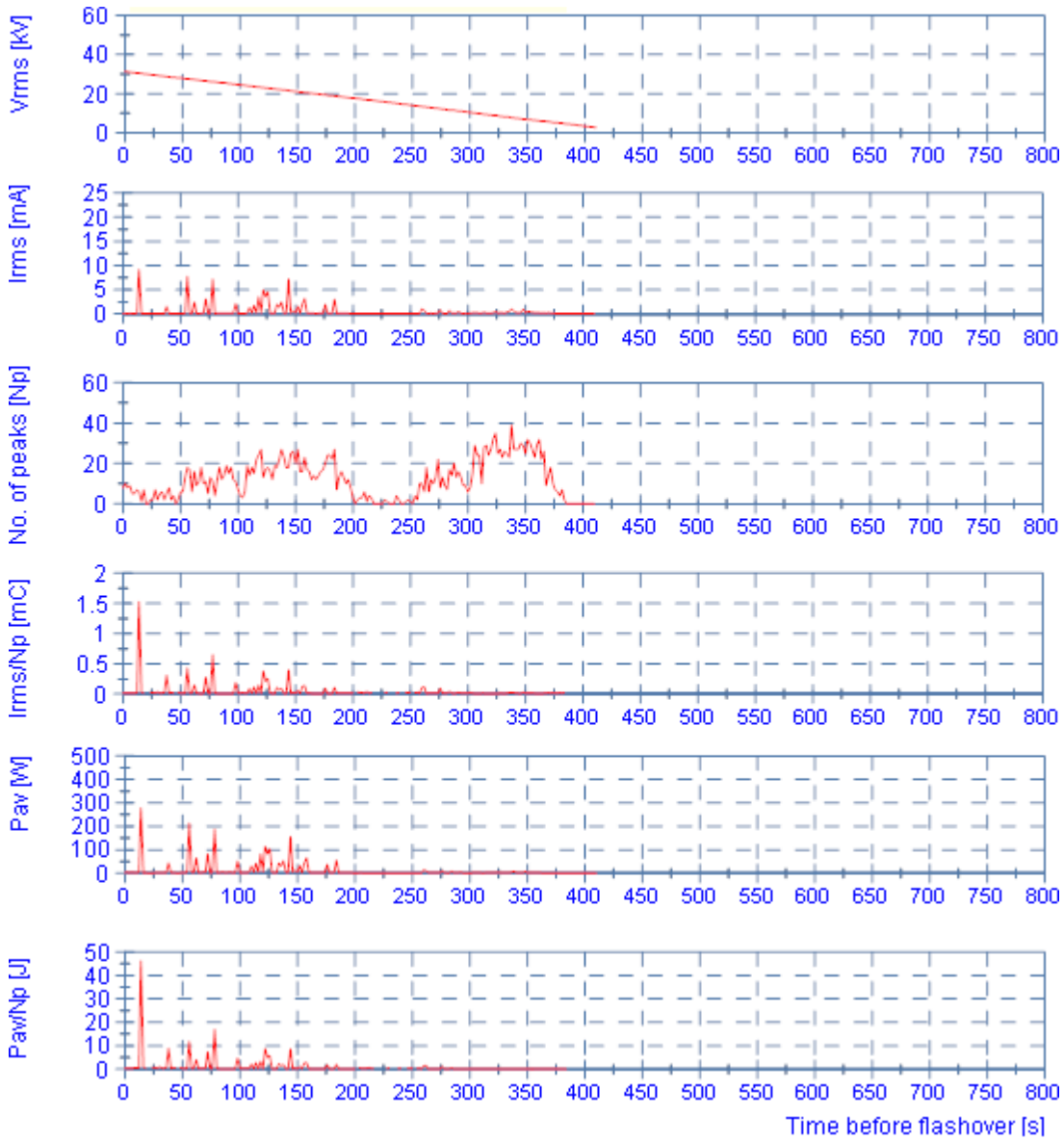

Figure II.12c. *Analysis (2 s window) of ramp voltage data for a TT6B insulator, for high pollution (0.64 mg/cm2) and lower fog spray rate (3l/h) (3rd ramp). FOV 31.4 kV at 410 s.*

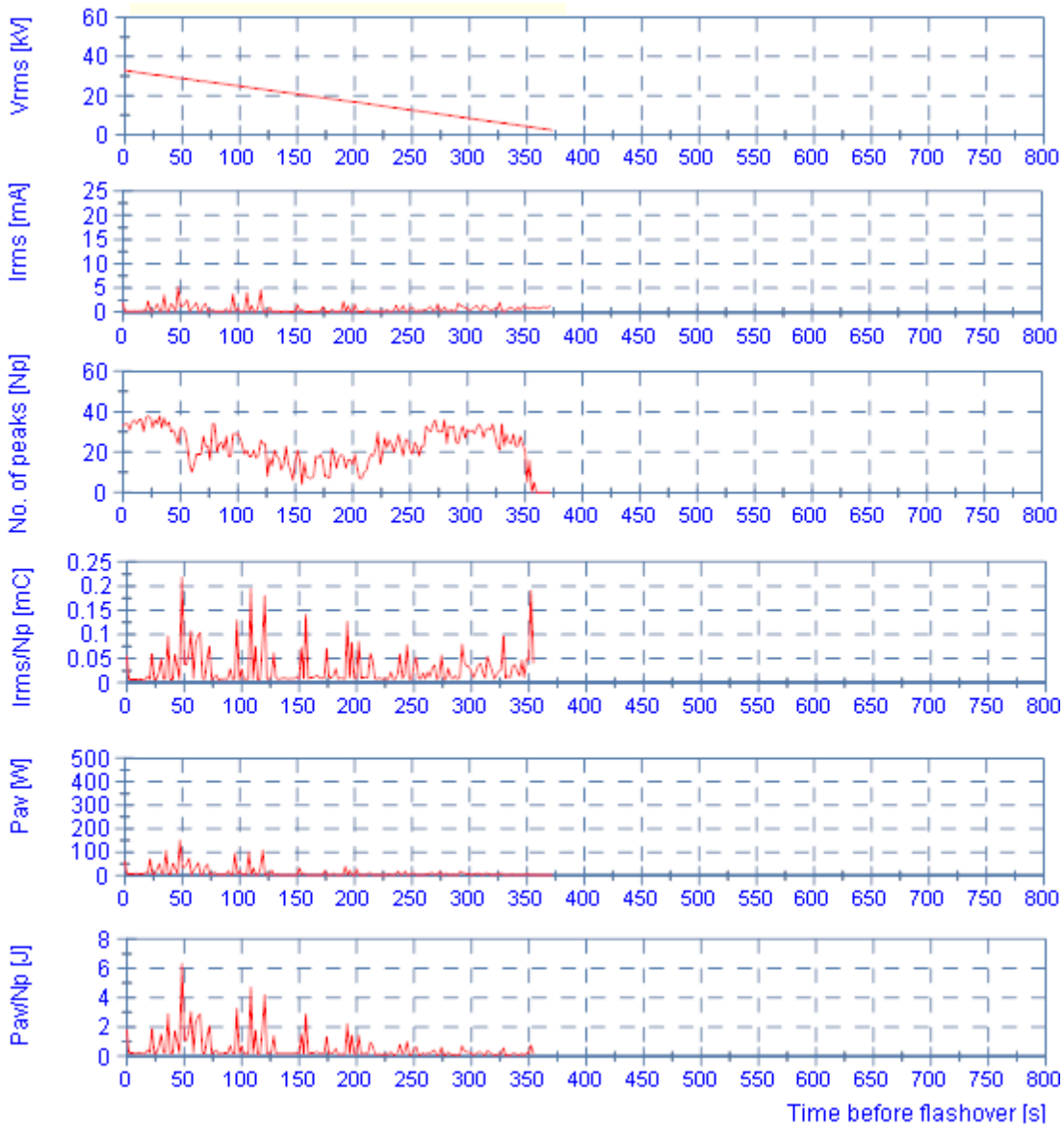

Figure II. 12d. *Analysis (2 s window) of ramp voltage data for a TTS6B insulator, for high pollution (0.64 mg/cm2) and lower fog spray rate (3l/h) (3rd ramp). FOV 32.9 kV at 372 s.*

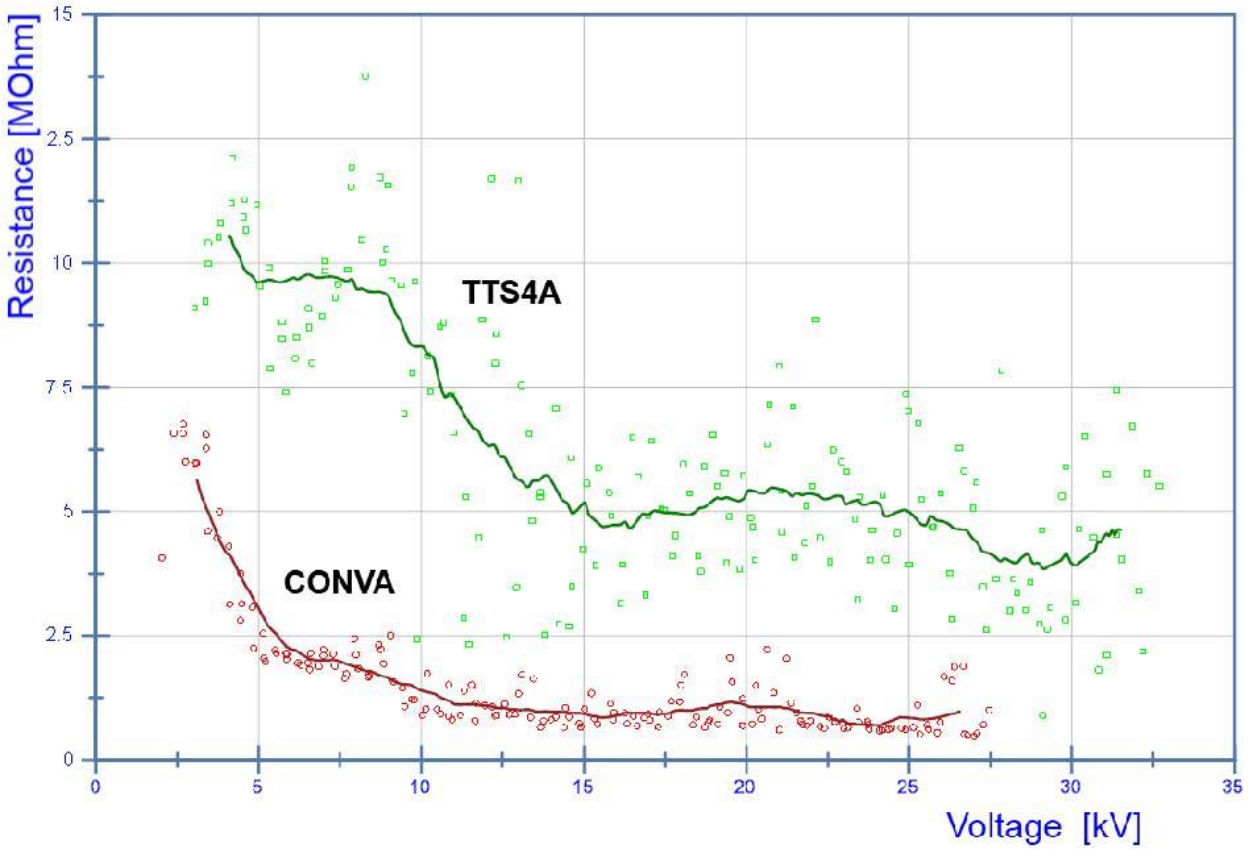

Figure II.13. *Leakage resistance during a ramp-voltage flashover test for CONVA and TSS4A insulators. Upper curve: CONVA. Lower curve: TTS4A. (0.64 mg/cm2, 8 l/h) 2 s sample window analysis.*

II.6 CONCLUSIONS

The recent IEC Technical Specification IEC/TS 60815 affirms the improved pollution withstand behaviour of HTM polymeric insulators such as silicone-rubber compared with glass and ceramic insulators of equal creepage distance. However, the specifications suggest that exploitation of this advantage in the dimensioning of silicone-rubber insulators is inadvisable if the site conditions put at risk the hydrophobicity to which this improvement is due. It further recommends that an even greater creepage distance than non-polymer insulators may be advisable in extreme cases. The present paper has introduced the design and prototype manufacture of silicone-rubber insulators with surface textures to provide increased creepage distance on the trunk and sheds. The enhanced clean-fog test procedures developed in Part 1 have been used to show that in this way the flashover voltage of an insulator with silicone-rubber of poor hydrophobicity is increased by up to 27% when severely polluted. The performance of insulators with a superior material can be matched by those of the low-hydrophobicity material when textures are employed. These tests have shown also that the higher flashover voltage of textured insulators is accompanied by, and arises from, a substantial reduction of the leakage current associated with local arcing. Importantly, this improvement in laboratory test performance of textured insulators over conventional insulators of the same profile is shown to increase with increasing pollution severity. This is valuable, because it is estimated that 5% of in-situ conditions for HVAC power systems present a risk of high conductivity pollutants and a permanent loss of hydrophobicity which have to be considered to limit insulator life. Field tests and commercial applications are under discussion.

.

CHAPTER III

EXPERIMENTAL STUDY AND RESULTS

Chapter III: Experimental Study and Results

III.1 Introduction

A novel design approach for polymer insulators, featuring a sequence of semi-elliptical surface protrusions, has been introduced to enhance insulation efficiency. This design aims to reduce energy dissipation by lowering both the electric field (E) and leakage current density (J), while also extending the longitudinal leakage path without increasing the overall insulator length. Furthermore, the creation of multiple parallel current paths can help minimize the impact of discharges. Preliminary findings indicate that this textured surface significantly outperforms conventional smooth-surface designs.

To assess the suitability of materials for outdoor insulation applications, it is essential to evaluate their resistance to abrasion and surface tracking. The inclined plane test serves as a standardized accelerated aging method, where flat samples are exposed to high-voltage stress conditions to simulate long-term degradation due to corrosion and tracking. This chapter presents an experimental analysis of three PLA+ (polylactic acid plus) samples—each with a distinct surface texture: non-textile, transversely textile, and longitudinally textile for performance comparison under such conditions.

III.2 Experimental Setup

III.2.1 High Voltage Laboratory Test Circuit (University of El Oued)

The tests are conducted in the high voltage laboratory at the University of El Oued.

Our laboratory is equipped with three voltage sources:

• A power supply with an industrial frequency of 50Hz.

• A DC voltage generator.

• An impulse voltage generator.

III.2.1.1 Test Station Equipment

The test station in our laboratory comprises the following components:

- A test transformer.
- A regulating transformer.
- Voltage dividers.
- A control panel with measuring and protective devices.
- A digital oscilloscope.
- Conductivity measuring device.

III.2.1.2 Test Transformer

We used a test transformer designed and insulated for high-voltage generation. It has a transformation ratio of 250V/100kV, with a power rating of 5 kVA. This transformer allows the high voltage at the secondary side to be varied from 0 to full voltage.

III.2.1.3 Regulating Transformer

We allow for the variation of the voltage at the terminals of the test transformer. Its transformation ratio is 220V/250V.

III.2.1.4 Digital Oscilloscope

It is a device that allows for the visualization of waveforms and recorded phenomena (Figure III.1).

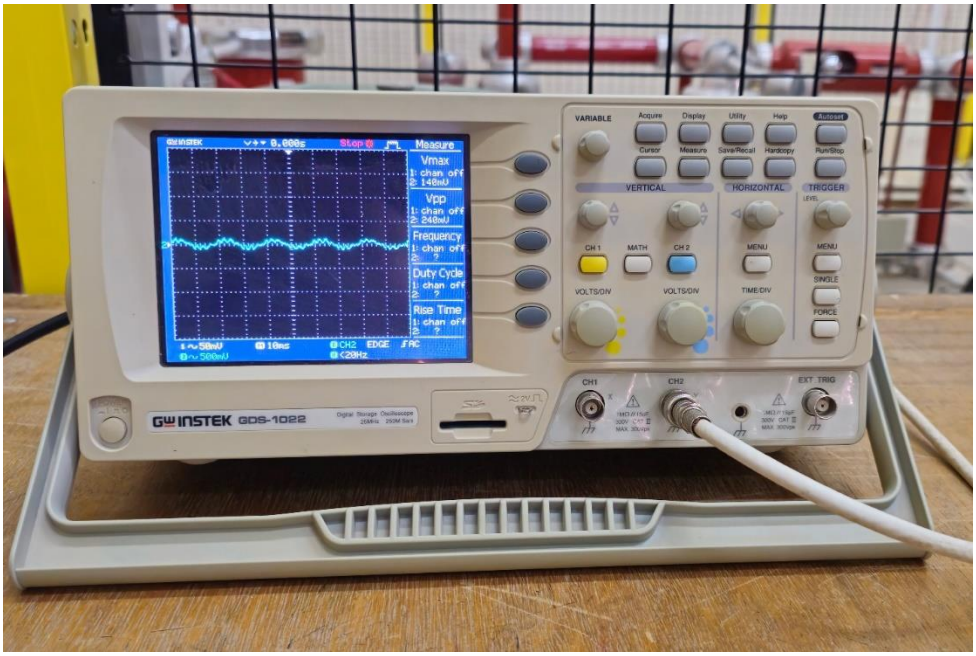

Figure III.1. *Digital Oscilloscope.*

III.2.1.5 Control Panel

This panel is powered by a 220V supply. It allows for the automatic variation of the test voltage. See Figure (III.2).

Figure III.2. *Photo of the control panel in the high voltage laboratory at the University of El Oued.*

III.2.1.6 Measurement and Protection Devices

The laboratory power supply is controlled from a control panel located in the laboratory outside the test platform (the Faraday cage). The high-voltage transformer and its regulator are independently protected by a 250A fuse and a thermal relay. These protections are connected to the main contactor coil circuit, providing sufficient protection against transformer overloads and short-circuit currents.

For voltage measurements, we have:

• DSM: a digital voltmeter for measuring alternating voltage.

• DGM: a digital voltmeter for measuring direct voltage.

• A voltmeter and ammeter for measuring primary voltage at the test transformer.

III.2.1.7 Voltage Divider

There are two types of voltage dividers:

• A capacitive voltage divider for measuring industrial frequency voltage.

• A resistive voltage divider for measuring DC voltage.

III.2.1.8 Alternating Voltage Test Circuit

High-voltage alternating current generators, operating at frequencies between a few Hz and 1 kHz, generally use step-up transformers.

High-voltage alternating current generators are used for:

• High-voltage alternating current tests (high-voltage transformers).

• Power supply (high-voltage transformers) for DC rectifiers, oscillating circuit generators, and impulse generators.

Figure III.3 shows the alternating voltage test circuit realized in the high-voltage laboratory, and Figure III.4 is a corresponding photo of the setup in the high-voltage laboratory.

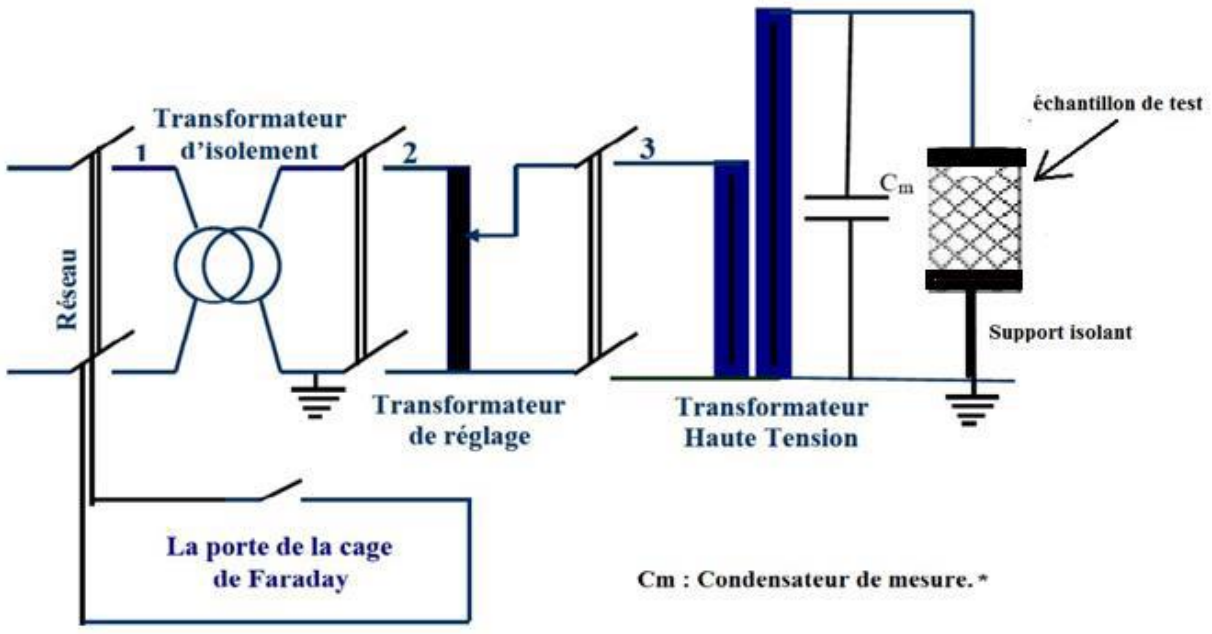

Figure III.3. *Industrial Frequency Test Circuit.*

Figure III. 4. *Photo of the Industrial Frequency Test Circuit.*

III.3 Operating mode

Most studies consider experimental models of simple geometry and rarely the profile of a real insulator. However, while these equivalent models do not exactly reflect the behavior of real insulators, they allow for a better visualization of the electrical discharge phenomenon.

III.3.1 Experimental model

Rectangular PLA+ samples were made. The dimensions were 120 mm x 48 mm x 5 mm. Three samples were prepared. See Figure 5.

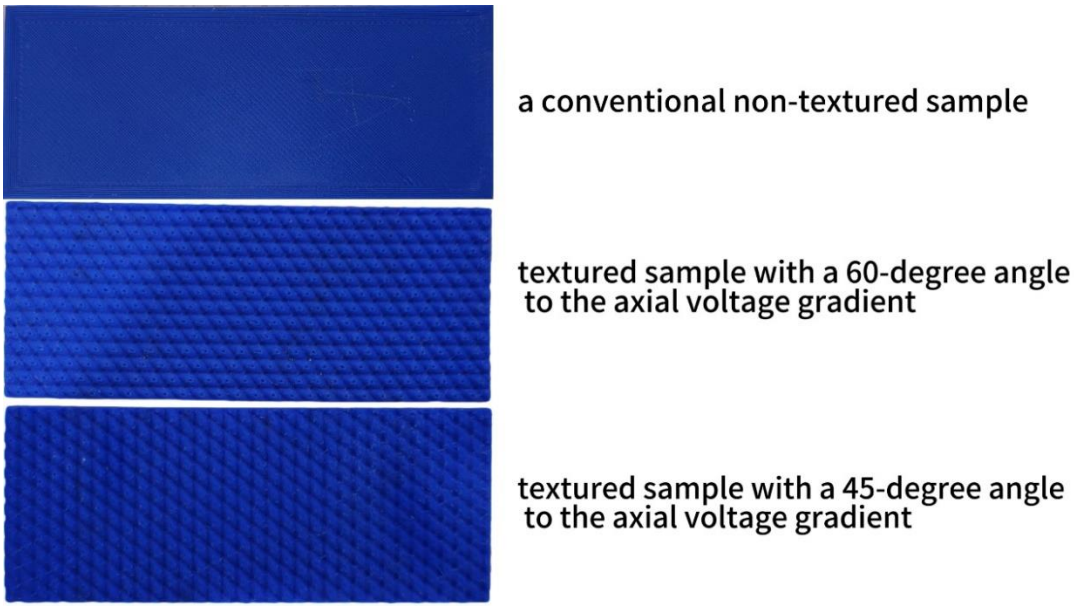

Figure III.5. *Three samples: a traditional non- textured sample and two woven samples*

III.3.2 Preparation of the model

Before each series of tests, the insulating panel is carefully cleaned and then soaked in gas oil in the areas where the galvanized steel electrodes will be placed to ensure close contact between the panel and the electrodes without leaving any gaps. The panel is then wiped with cotton soaked in alcohol to remove any residue of gas oil from the insulating surface. We then installed aluminum foil on the insulator as electrodes, changing the distance between them 4 cm , 8 cm, in all three cases: non- textured, textured with a 60 degree angle, and textured with a 45 degree angle.

III.4 Test Procedure

The objective of these tests is to study how the leakage current and the flashover voltage evolve based on the applied electro-geometric parameters on the laboratory model.

III.4.1 Flashover Voltage Measurement

The determination of the flashover voltage (representing the arithmetic mean of three values) from the two samples. These measurements determine the limit voltage levels that will be applied to measure the leakage current.

III.4.2 Leakage Current Measurement

For different levels ranging from 5 kV to 20 kV in steps of 5 kV, and for each configuration, the amplitude of the leakage current is determined by measuring the voltage across a non-inductive

10 KΩ resistor inserted in the earth return. For this, we used a memory oscilloscope with a bandwidth of 25 MHz. To avoid any influence of noise in the captured signal, we place the resistor in an aluminum metal box grounded, thus forming an electrostatic shield.

III.4.3 Atmospheric Correction

For each test conducted, the atmospheric conditions are recorded using a special electronic Device.

III.4.3.1 Influence of Air Relative Density

Temperature and pressure influence the dielectric strength of air. In IEC 60 (International Electrotechnical Commission), we find the concept of relative density, which is defined as the ratio of the density of air under given pressure (P) and temperature (T) conditions to the density of air under standard atmospheric conditions, i.e.:

- Ambient temperature T0 = 28°C.

- Atmospheric pressure P0 = 1008 mbar (= 756 mm Hg).

$$\partial = \frac{293}{760} * \frac{P}{(273+T)} \quad \textbf{(10)}$$

∂ is the correction factor for air density.

The pressure P is in mbar and the temperature T is in °C.

This equation is used to convert the measured discharge voltage Um under test atmospheric conditions (temperature T and pressure P) to the value Ucr that would have been obtained under standard conditions (T0 and P0):

$$\text{Ucr} = \frac{Um}{\partial} \leq 1 \quad (10)$$

III.4.3.2 Influence of Humidity

In the case of fast or very fast waves, such as those caused by lightning, the breakdown voltage is less sensitive to humidity variations. Therefore, during our tests, where the relative humidity varied between 34% and 56%, we did not take this aspect into account.

III.5 Experimental Results

III.5.1 The non- textured sample [33]

The following table represents the variations in flashover voltage and the effect of corona and partial discharge in the case of the non- textured sample with adjustment of the distance between the electrodes. Additionally, it includes selected real images during the experiment.

Table III.1. The table represent changes in voltage across the non- textured sample varying distance between the electrodes.

		1	2	3	Average	Corrected
The distance between the electrodes is 4 cm	Corona effect	15.50	15.86	14.86	15.40	14.9
	Flashover voltage	34.61	34.50	34.20	34.43	33.3
The distance between the electrodes is 8 cm	Corona effect	29.35	30.00	31.21	30.18	29.18
	Flashover voltage	57.54	57.60	58.31	57.81	55.9

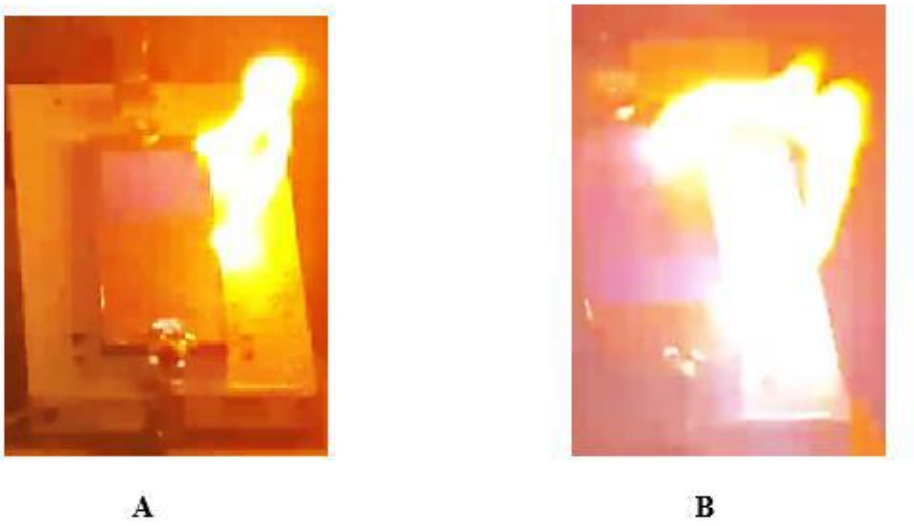

Figure III .7. *Real images of the flashover voltage variation in the non- textured sample at different distance between the electrodes: (A) 4cm, (B) 8 cm.*

III.5.2 A 60 Degree Textured Sample

The following table represents the variations in flashover voltage and the effect of corona and partial discharge in the case of the 60 Degree textured sample with adjustment of the distance between the electrodes. Additionally, it includes selected real images during the experiment.

Table III.2. The table represent changes in voltage across 60 Degree Textured Sample at varying distance between the electrodes.

		1	2	3	Average	Corrected
The distance between the electrodes is 4 cm	Corona effect	30.09	30.59	29.32	30.00	28.8
	Flashover voltage	39.05	40.10	38.50	39.21	37.64
The distance between the electrodes is 8 cm	Corona effect	30.25	33,50	32.50	32.08	31.48
	Flashover voltage	61.32	60.09	59.31	57.90	58.25

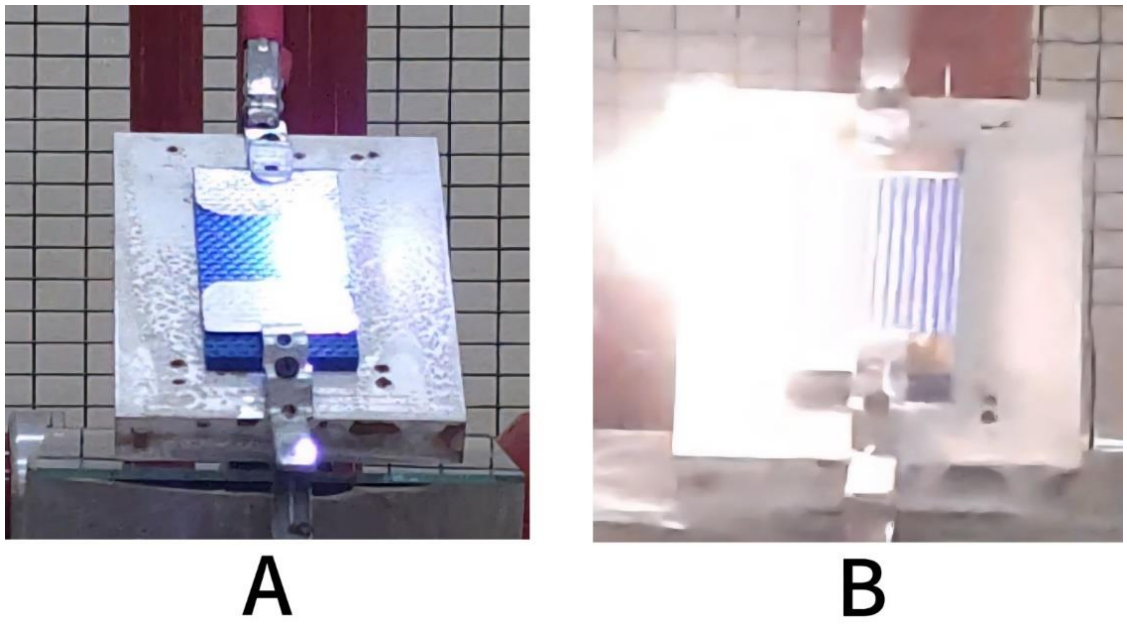

Figure III. 9. *Real images of the flashover voltage variation in 60 Degree Textured Sample at varying distance between the electrodes: (A) 4cm, (B) 8 cm.*

III.5.3 A 45 Degree Textured Sample

The following table represents the variations in flashover voltage and the effect of corona and partial discharge in the case of the 45 Degree textured sample with adjustment of the distance between the electrodes. Additionally, it includes selected real images during the experiment.

Table III.3. The table represent changes in voltage across 45 Degree Textured Sample at varying distance between the electrodes.

		1	2	3	Average	Corrected
The distance between the electrodes is 4 cm	Corona effect	25.03	25.6	26.04	25.55	24.70
	Flashover voltage	39.44	40.61	39.75	39.93	38.61
The distance between the electrodes is 8 cm	Corona effect	28.5	29.05	29.03	28.86	27.90
	Flashover voltage	66.09	64.5	65.85	65.48	63.32

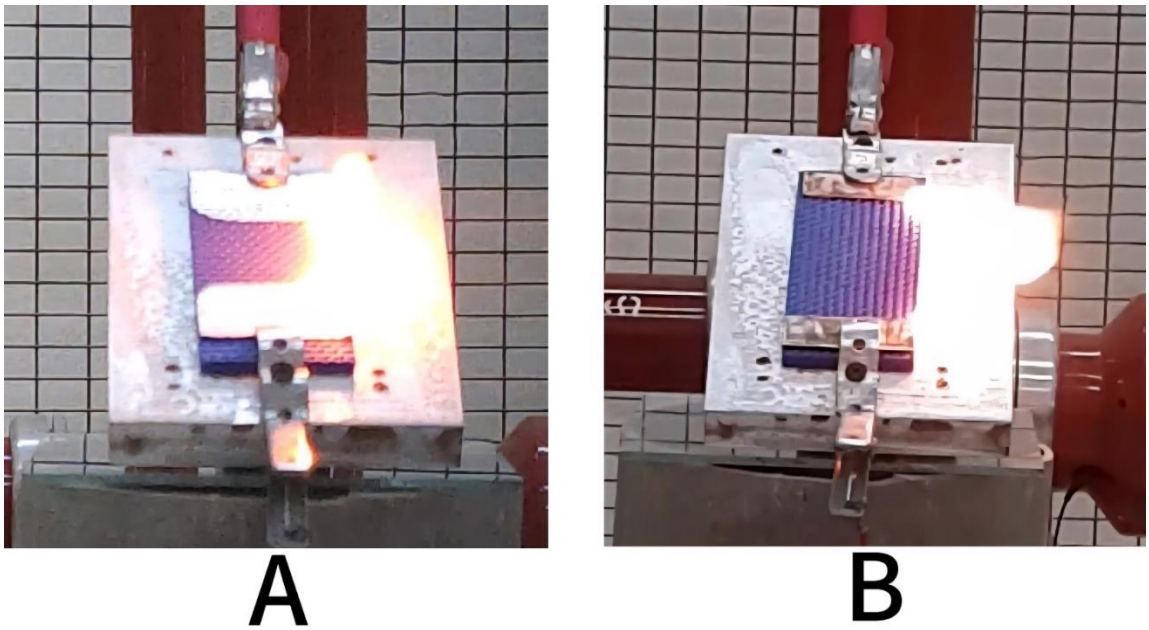

Figure III. 9. *Real images of the flashover voltage variation in 45 Degree Textured Sample at varying distance between the electrodes: (A) 4cm, (B) 8 cm.*

III.5.4 Longitudinally Textured Sample [33]

The following table represents the variations in flashover voltage and the effect of corona and partial discharge in the case of the Longitudinally textured sample with adjustment of the distance between the electrodes. Additionally, it includes selected real images during the experiment.

Table III.2. The table represent changes in voltage across Longitudinally Textured Sample at varying distance between the electrodes.

		1	2	3	Average	Corrected
The distance between the electrodes is 4 cm	Corona effect	16.68	18.55	20.45	18.56	17.81
	Flashover voltage	38.65	35.34	36.96	36.98	35.50
The distance between the electrodes is 8 cm	Corona effect	24.20	25.10	25.25	24.85	23.85
	Flashover voltage	64.85	65.19	64.18	64.73	62.14

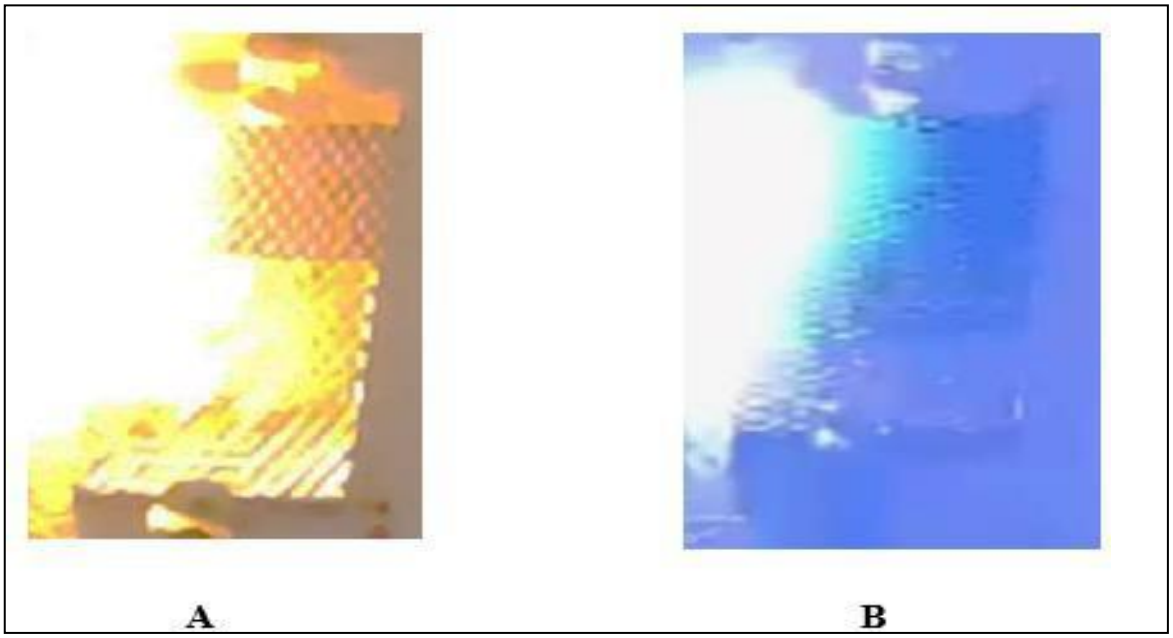

Figure III. 9. *Real images of the flashover voltage variation in the Longitudinally textured sample at different distance between the electrodes : (A) 4cm, (B) 8 cm.*

III.5.5 Transversely Textured Sample [33]

The following table represents the variations in flashover voltage and the effect of corona and partial discharge in the case of the Transversely textured sample with adjustment of the distance between the electrodes. Additionally, it includes selected real images during the experiment.

Table III.3. The table represent changes in voltage across Transversely Textured Sample at varying dimension between the electrodes.

		1	2	3	Average	Corrected
The distance between the electrodes is 4 cm	Corona effect	22.86	23.41	22.50	22.92	22.00
	Flashover voltage	36.22	36.55	36.87	36.54	35.07
The distance between the electrodes is 8 cm	Corona effect	27.56	29.36	28.41	28.44	27.30
	Flashover voltage	62.41	61.53	63.37	62.43	59.93

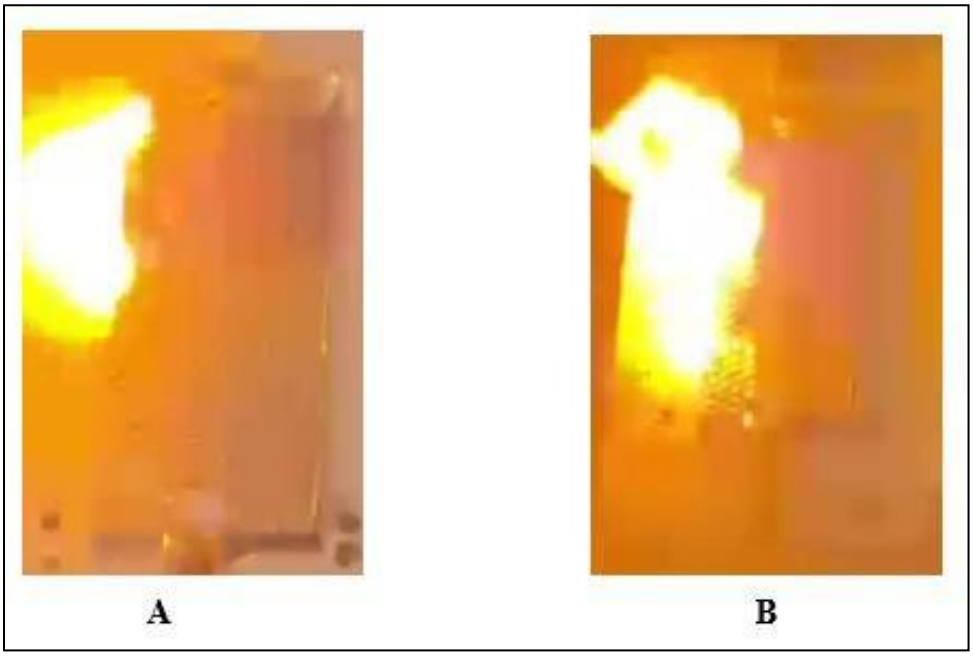

Figure III.11. *Real images of the flashover voltage variation in the Transversely textured sample at different distance between the electrodes : (A) 4cm, (B) 8 cm.*

III.5.6 Leakage current

Here we are studying the effect of samples on the value of leakage current. Therefore, different voltage levels and distances were considered.

$$\mathbf{I} = \frac{\mathbf{U}}{\mathbf{R}} \ /\mathrm{R} = 10\ \mathrm{K}\Omega \qquad \textbf{(12)}$$

III.5.6.1 The non- textured sample [33]

Table III.4. *The table represents the values of current leakage at different voltages*

Voltage (KV)	The distance between the electrodes is 4 cm	The distance between the electrodes is 8 cm
	The current leakage value at different voltages(µA)	
2	10.01	8.90
5	12.20	10.90
8	19.20	15

- <u>The distance between the electrodes is 4 cm</u>

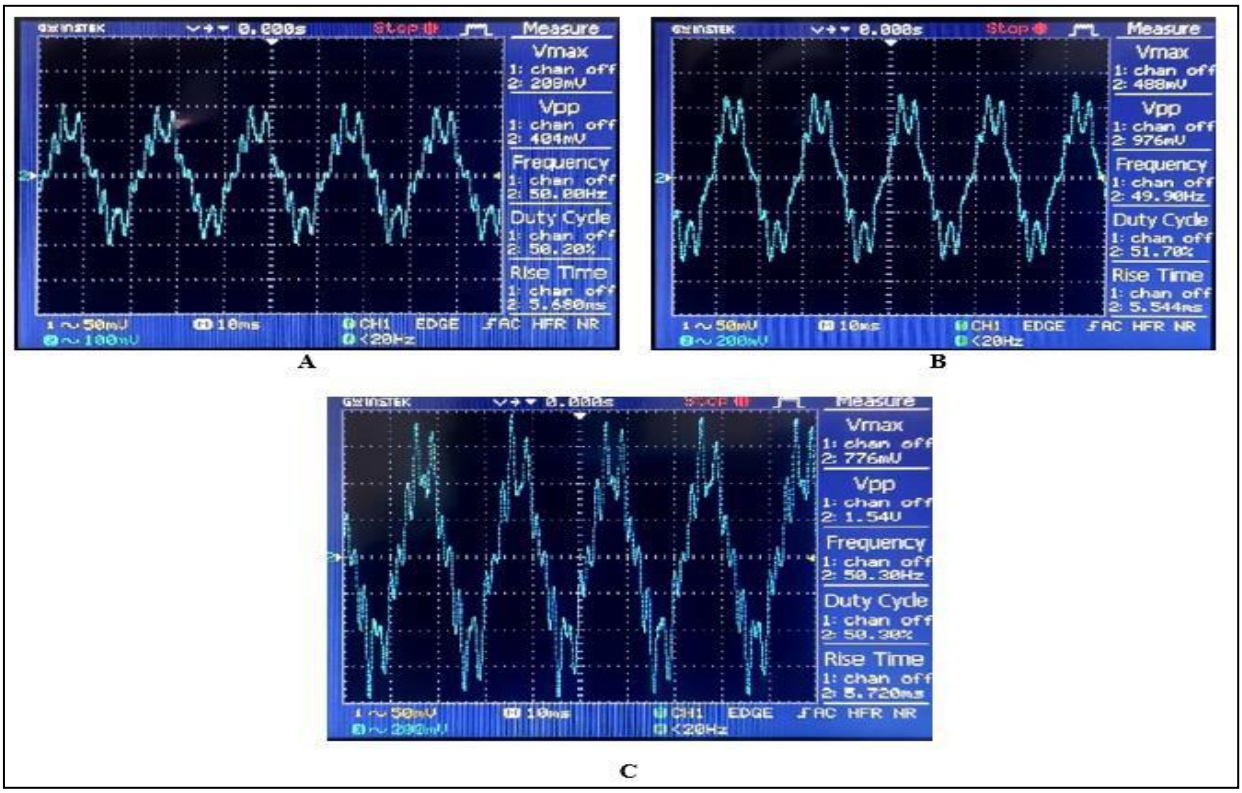

Figure III.14. *Graphical curves of leakage current for the non- textured sample under different voltages: (A) 2KV, (B) 5KV, (C) 8KV.*

- **The distance between the electrodes is 8 cm**

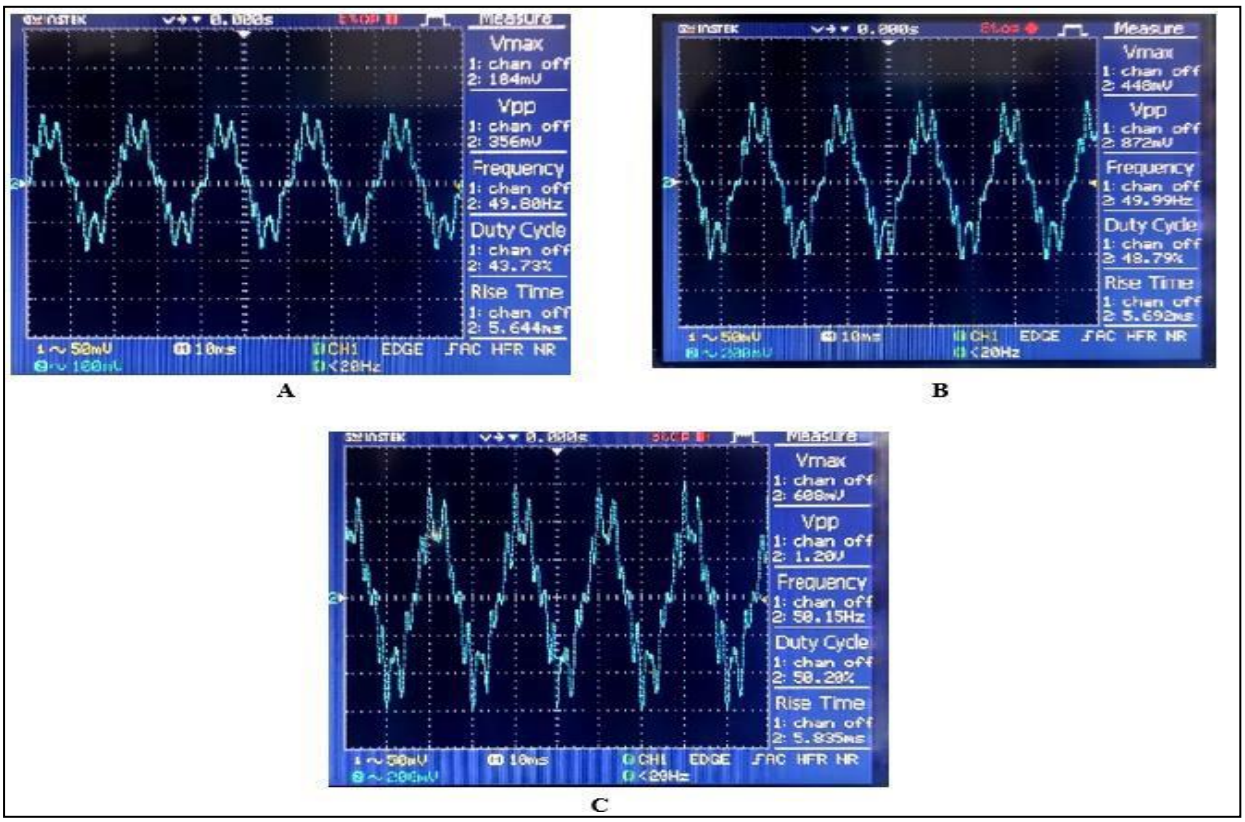

Figure III.15. *Graphical curves of leakage current for the non- textured sample under different voltages: (A) 2KV, (B) 5KV, (C) 8KV.*

III.5.6.2 Textured sample with a 60-degree angle

Table III.4. *The table represents the values of current leakage at different voltages*

Voltage (KV)	The distance between the electrodes is 4 cm	The distance between the electrodes is 8 cm
	The current leakage value at different voltages(µA)	
2	1.18	0.71
5	3.1	1.98
8	5.25	3.26

• **The distance between the electrodes is 4 cm**

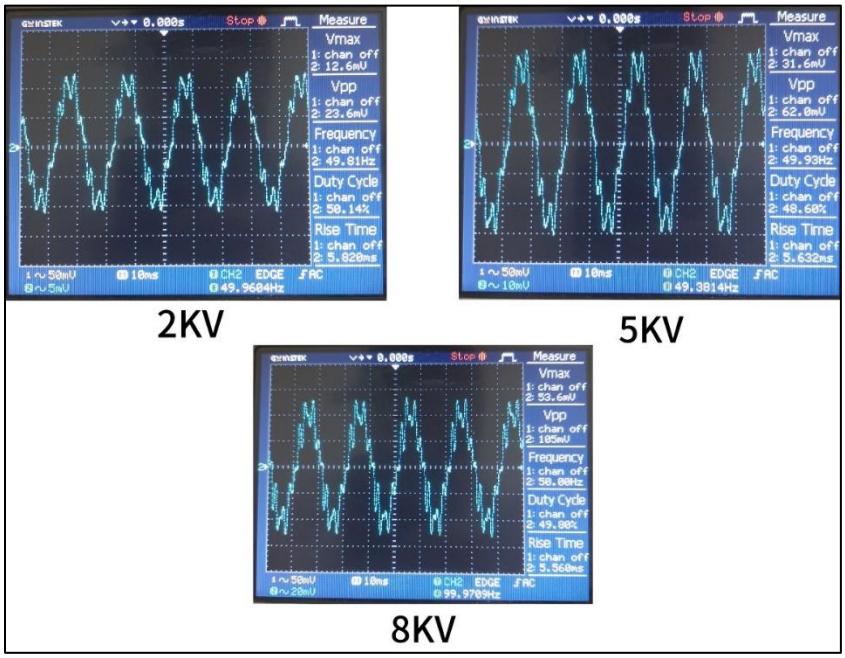

Figure III.14. *Graphical curves of leakage current for Textured sample with a 60-degree angle under different voltages: (A) 2KV, (B) 5KV, (C) 8KV.*

• **The distance between the electrodes is 8 cm**

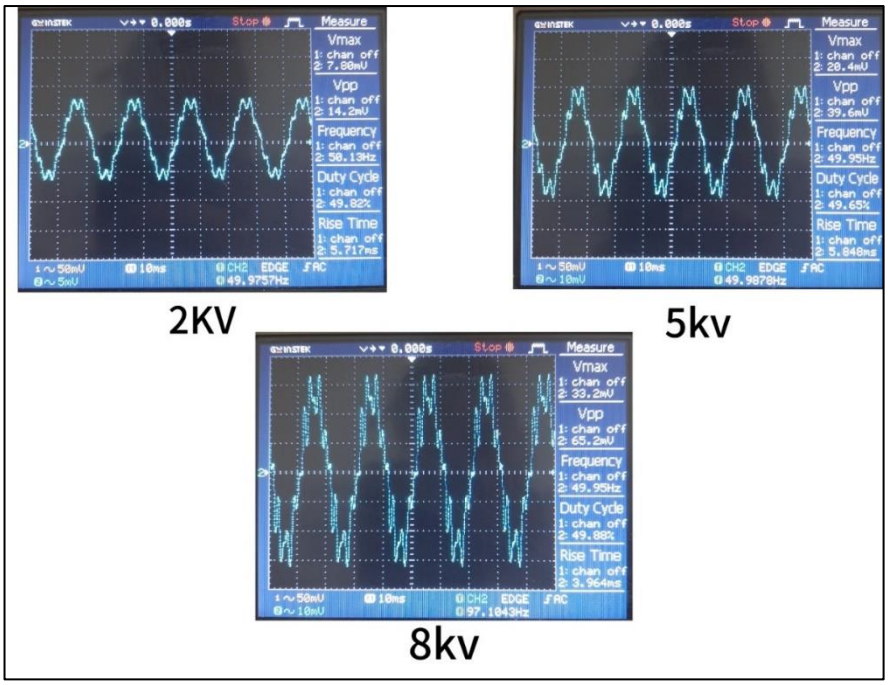

Figure III.14. *Graphical curves of leakage current for Textured sample with a 60 degree angle under different voltages: (A) 2KV, (B) 5KV, (C) 8KV.*

III.5.6.3 Textured sample with a 60-degree angle

Table III.4. The table represents the values of current leakage at different voltages

Voltage (KV)	The distance between the electrodes is 4 cm	The distance between the electrodes is 8 cm
	The current leakage value at different voltages(µA)	
2	1.56	1.5
5	3.36	2.68
8	5.2	4.44

- **The distance between the electrodes is 4 cm**

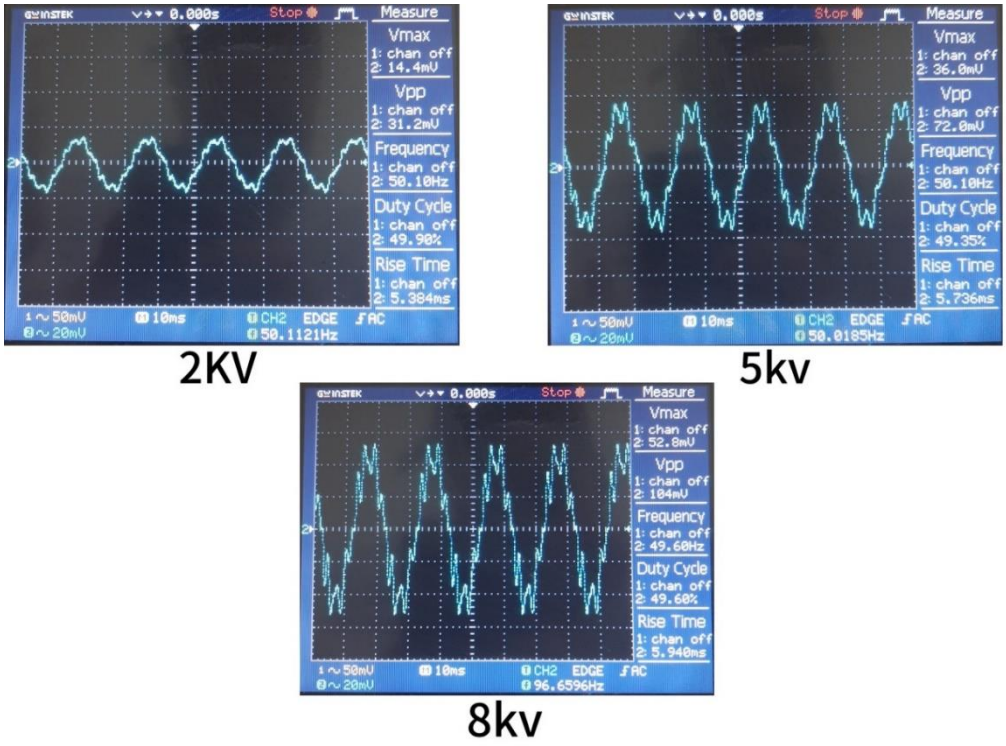

Figure III.14. *Graphical curves of leakage current for Textured sample with a 45 degree angle under different voltages: (A) 2KV, (B) 5KV, (C) 8KV.*

- **The distance between the electrodes is 8 cm**

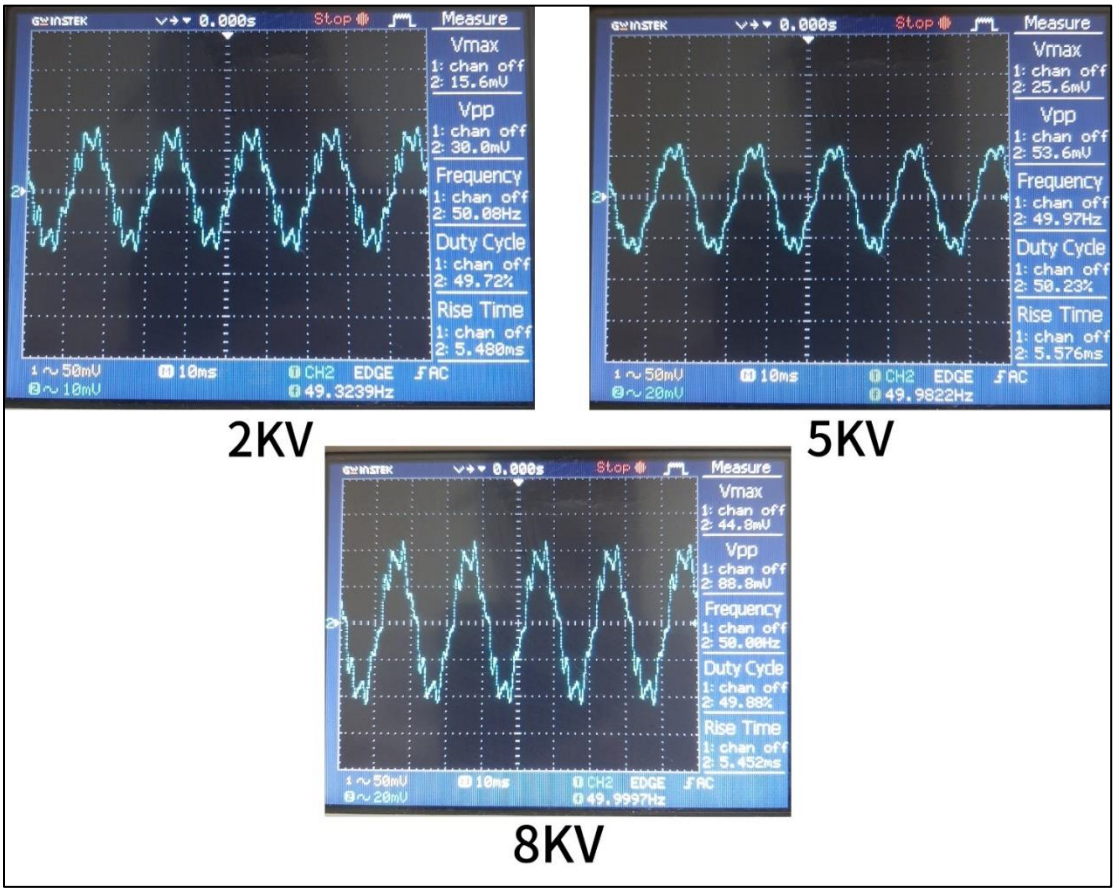

Figure III.14. *Graphical curves of leakage current for Textured sample with a 45 degree angle under different voltages: (A) 2KV, (B) 5KV, (C) 8KV.*

III.5.6.4 Longitudinally Textured Sample [33]

Table III.5. The table represents the values of current leakage at different voltages

Voltage (KV)	The distance between the electrodes is 4 cm	The distance between the electrodes is 8 cm
	The current leakage value at different voltages(μA)	
2	1.20	1.32
5	2.80	3.08
8	4.8	5.3

- **The distance between the electrodes is 4 cm**

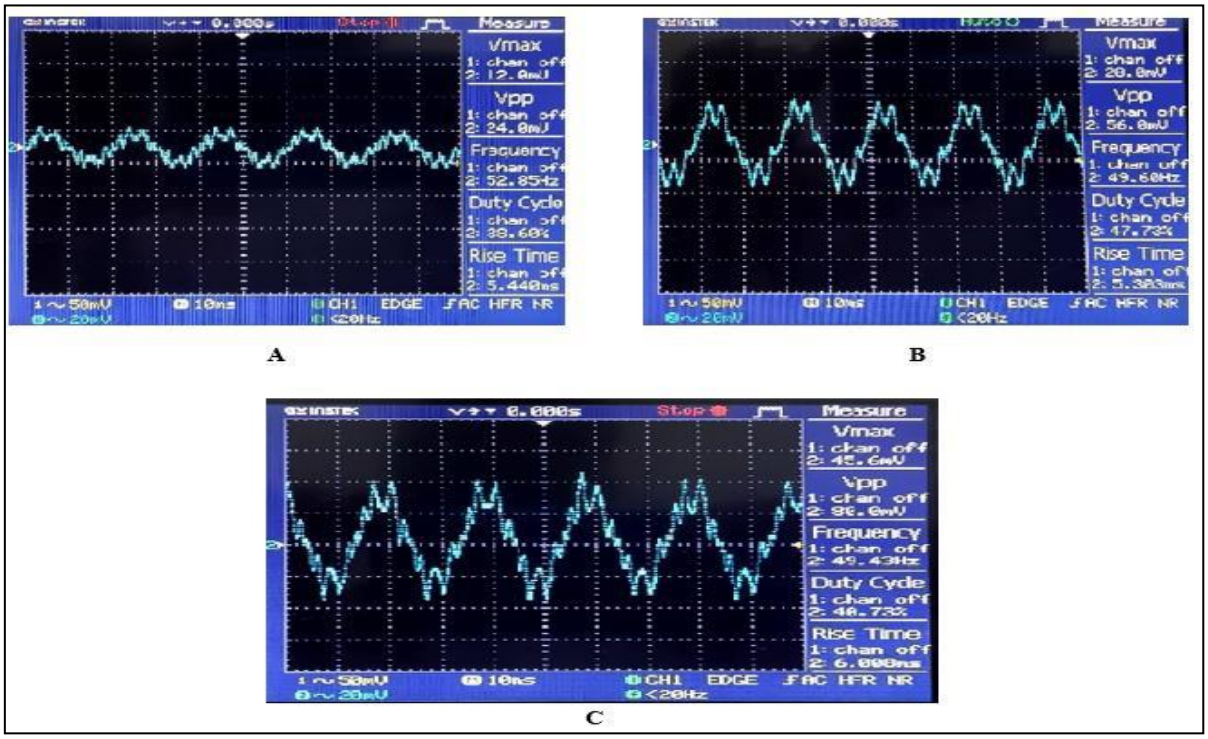

Figure III. 16.*Graphical curves of leakage current for the Longitudinally textured sample under different voltages: (A) 2KV, (B) 5KV, (C) 8KV.*

- **The distance between the electrodes is 8 cm**

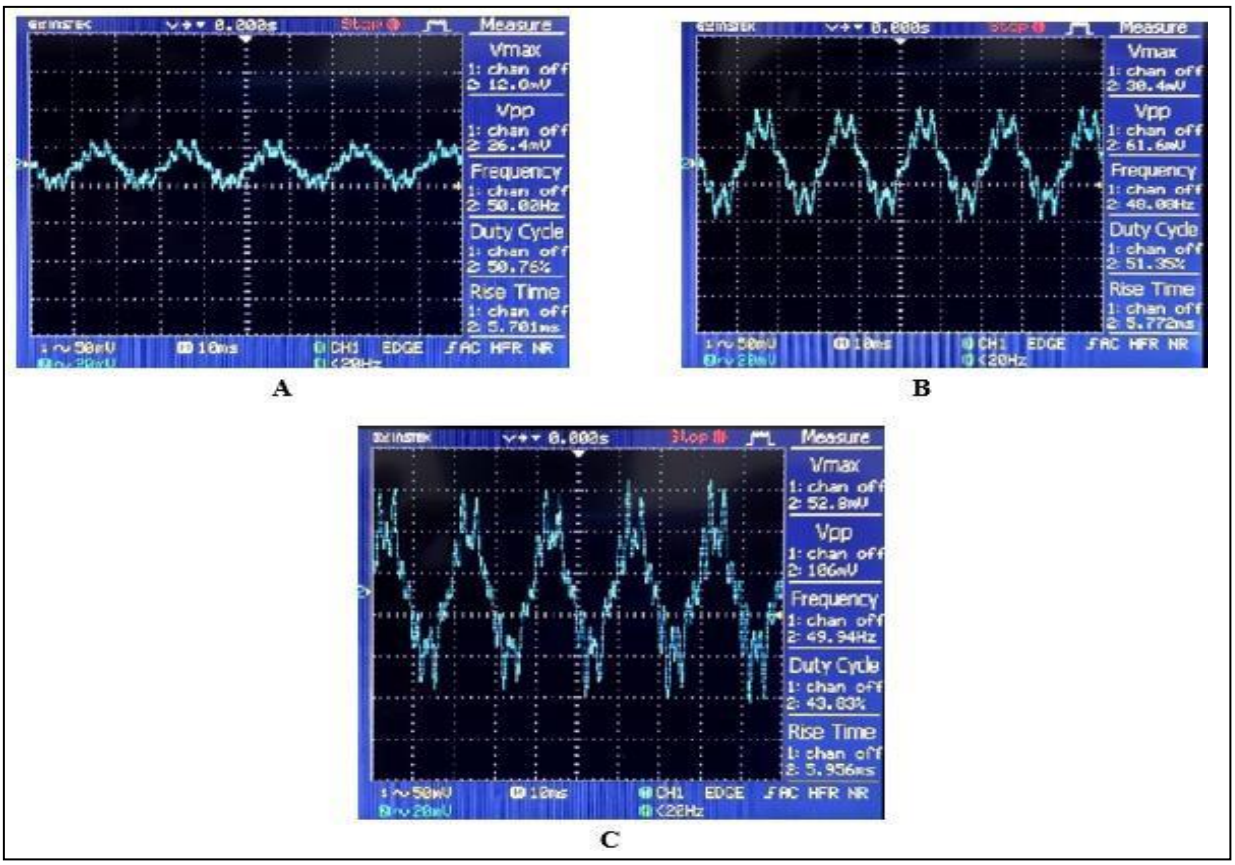

Figure III.17. *Graphical curves of leakage current for the Longitudinally textured sample under different voltages: (A) 2KV, (B) 5KV, (C) 8KV.*

III.5.6.5 Transversely Textured Sample [33]

Table III.6. Table III.6. The table represents the values of current leakage at different voltages

Voltage (KV)	The distance between the electrodes is 4 cm	The distance between the electrodes is 8 cm
	The current leakage value at different voltages(µA)	
2	1.20	1.10
5	3.08	2.40
8	5.30	4.50

- **The distance between the electrodes is 4 cm**

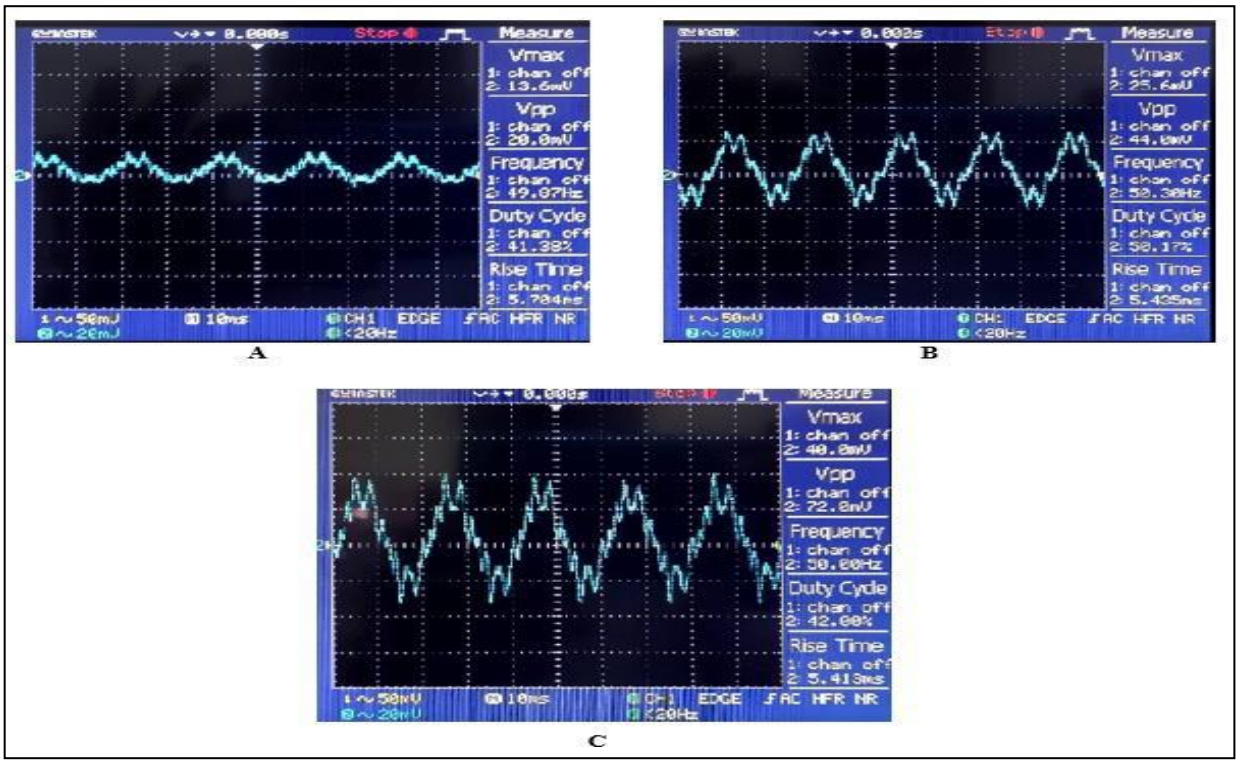

Figure III.18. *Graphical curves of leakage current for the Transversely textured sample under different voltages: (A) 2KV, (B) 5KV, (C) 8KV.*

- **The distance between the electrodes is 8 cm**

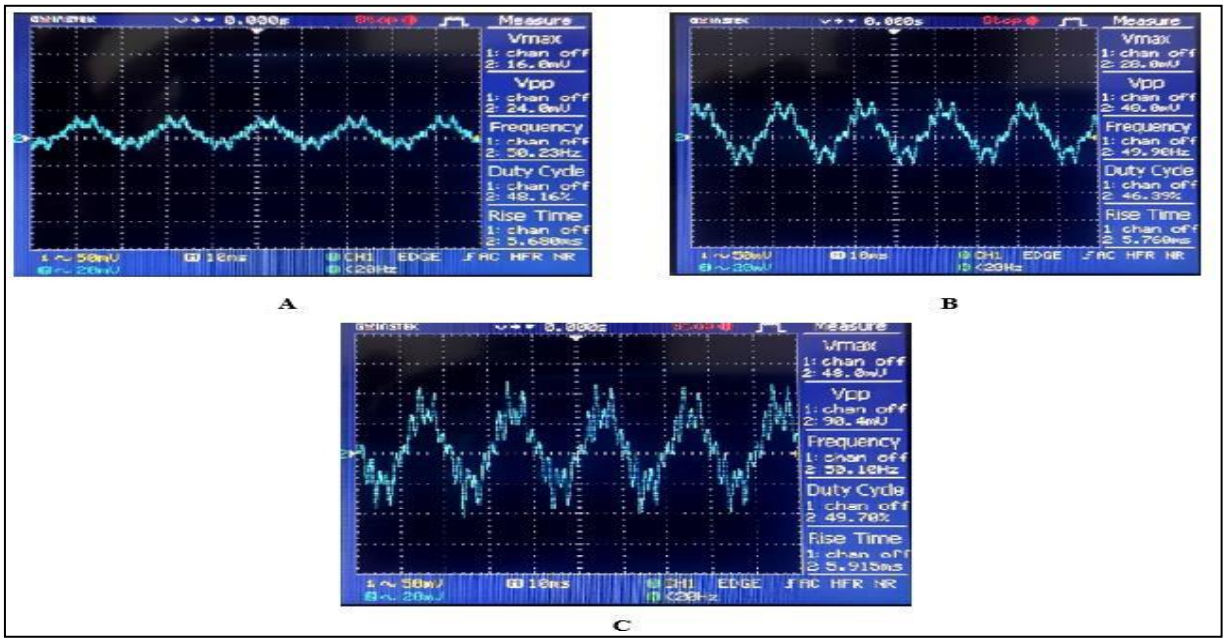

Figure III.19. *Graphical curves of leakage current for the Transversely textured sample under different voltages: (A) 2KV, (B) 5KV, (C) 8KV.*

III.5.7 Final Extraction

1. **Flashover Performance**:
    - The **45° textured sample** delivered the **highest flashover voltage**, outperforming non-textured surfaces by over **13%** at larger electrode gaps.
    - All textured patterns improved FOV, with better performance at **larger distances** due to extended leakage paths.
2. **Leakage Current Suppression**:
    - The **60° texture** most effectively reduced leakage current, showing more than **80% improvement** over the non-textured sample at comparable voltages.
3. **Best Overall Pattern**:
    - If optimizing for **flashover resistance**, the **45° textured surface** is superior.
    - If minimizing **leakage current**, **60° texturing** yields the best results.
    - Therefore, the **45° texture** presents a balanced solution offering **both strong FOV and good current suppression**.

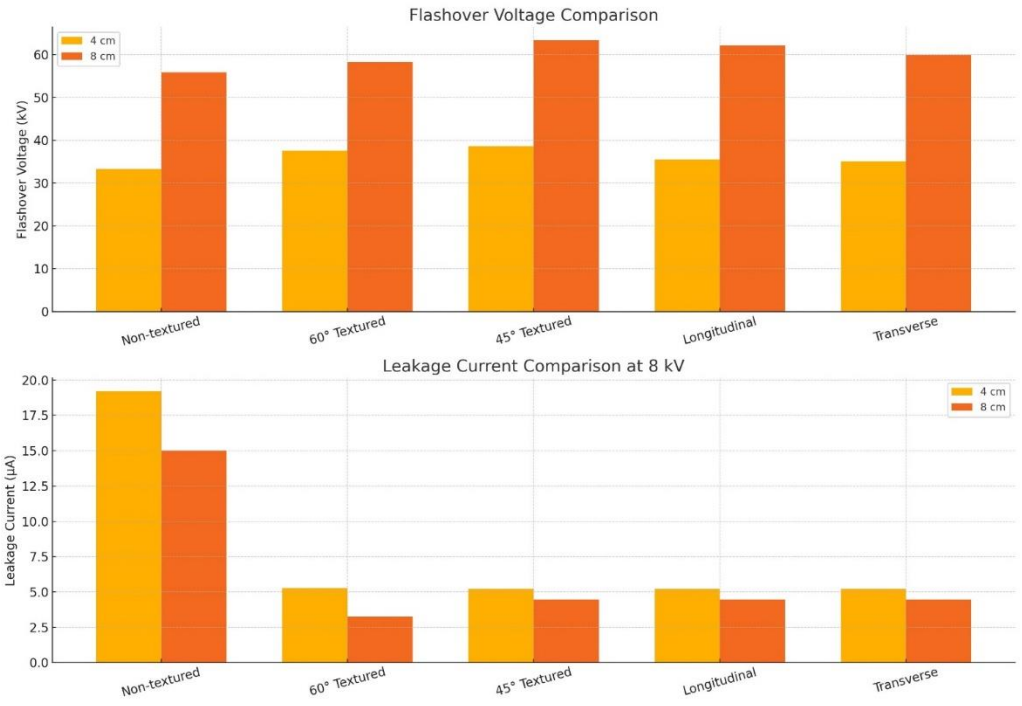

FigureIII.20 Comparison of Flashover Voltage and Leakage Current for Textured and Non-Textured Insulator Samples

III.6 Conclusion

This chapter presented a comprehensive experimental investigation into the impact of surface texturing on the performance of polymeric insulators, focusing on flashover voltage and leakage current characteristics under varying electro-geometric conditions.

Three different PLA+ sample configurations were examined: non-textured, 60° textured, and 45° textured, in addition to longitudinally and transversely textured samples. The tests were conducted using a standardized high-voltage laboratory setup under controlled environmental conditions.

The results clearly demonstrate that surface texturing significantly enhances insulator performance:

- The flashover voltage increased across all textured samples compared to the non-textured reference, with the 45° textured pattern showing the most notable improvement. This is attributed to the elongated creepage paths and the creation of multiple discharge-interrupting surface features.
- Leakage current was substantially reduced in all textured samples. The 60° textured pattern achieved the lowest leakage values, indicating effective suppression of current conduction paths along the surface.
- The longitudinally and transversely textured samples also exhibited enhanced performance, with higher flashover thresholds and reduced current densities, validating the benefit of directional surface engineering.

Overall, these findings confirm that introducing strategic surface textures is a promising approach to improving the reliability and durability of high-voltage polymeric insulators. The results support the use of 45° and 60° textured configurations in environments prone to pollution and moisture, offering a practical solution for reducing maintenance and increasing the lifespan of outdoor insulation systems

GENERAL CONCLUSION

General Conclusion

High-voltage insulators are indispensable components in electrical power systems, serving to maintain insulation integrity under a wide range of environmental and operational stresses. This work has addressed the performance limitations of conventional insulators under polluted conditions and presented innovative solutions based on surface engineering.

In **Chapter I**, we established a comprehensive foundation on the various types of high-voltage insulators, their materials (ceramic, glass, polymer), and the detrimental effects of environmental pollution. The chapter highlighted how surface contamination, when combined with moisture, can lead to leakage currents and ultimately flashover events. The importance of selecting appropriate insulator types and profiles based on pollution severity was clearly emphasized.

Chapter II introduced a novel approach to mitigating pollution-induced flashover by employing **surface texturing** on polymeric insulators. Various texture geometries, including contiguous hemispherical and intersecting patterns, were analyzed for their ability to increase creepage distance and reduce electric field intensity. Theoretical modeling and laboratory simulations showed that surface textures not only increase the effective surface area but also create alternative current paths, reducing localized heating and dry-band formation. This significantly improves flashover voltage (FOV) and reduces leakage current, especially under high-pollution conditions.

Chapter III experimentally validated these theoretical findings through a series of tests on PLA+ samples with different textures and electrode spacings. The results confirmed that:

- **Textured insulators consistently outperform non-textured ones**, achieving higher flashover voltages and lower leakage currents.
- The **45° and 60° textures** demonstrated the best trade-off between electrical performance and surface engineering complexity.
- Surface textures act as a practical, low-cost solution to improving insulation performance, particularly in harsh environments where hydrophobicity may degrade over time.

REFERENCES

References

[1] M. S. Naidu & V. Kamaraju, *High Voltage Engineering* (5th ed.), McGraw-Hill Education, 2013.
– A foundational text covering principles of high voltage insulation, including materials and system design.

[2] D. Kind & K. Feser, *High Voltage Test Techniques* (2nd ed.), Newnes, 2001.
– Discusses the testing and behavior of high voltage insulators under operational stresses.

[3] IEC 60071-1, *Insulation Coordination – Part 1: Definitions, Principles and Rules*, International Electrotechnical Commission, 2019.
– Industry standard outlining insulation coordination, relevant to insulator design and selection.

[4] V. K. Mehta & R. Mehta, *Principles of Power System* (4th ed.), S. Chand Publishing, 2010.
– Provides a broad overview of power systems, including components like insulators and their roles in transmission.

[5] K. Chrzan & Z. Lubkowski, "Performance of High Voltage Composite Insulators in Polluted Environments," *IEEE Transactions on Dielectrics and Electrical Insulation*, vol. 19, no. 6, pp. 2103–2110, 2012.
– A research article on how modern composite insulators perform under environmental stresses.

[6] H. Salah Eddine & A. Mohamed Elfateh, *Estimation of the Flashover Voltage of a High Voltage Cap and Pin Insulator Artificially Polluted Using Fuzzy Logic*, Master's Thesis in Electrical Engineering, Mohamed Boudiaf University – M'Sila, 2019.
– A thesis exploring the use of fuzzy logic to estimate the flashover voltage of polluted high voltage insulators.

[7] R. S. Gorur, E. A. Cherney, & J. T. Burnham, *Outdoor Insulators*, USA: Ravi S. Gorur, 1999.
– A detailed reference on outdoor insulator performance, materials, aging, and field applications.

[8] J. S. T. Looms, *Insulators for High Voltages*, London, United Kingdom: Peter Peregrinus Ltd, 1988, pp. 2–12.
– A technical guide covering high voltage insulators, their design, and operational behavior.

[9] C. Bayliss & B. Hardy, *Transmission and Distribution Electrical Engineering*, Oxford, UK: Elsevier Ltd, 2007, pp. 163–168.
– A comprehensive textbook on electrical power transmission and distribution systems, including insulator applications.

[10] C.H.A. Ely, P.J. Lambeth, J.S.T. Looms, D.A. Swift, C.E.G.B., Bypassing of Wet and Polluted Polymers: The BOOSTER Shed, CIGRE, Report 15-02, Paris, France, 1978.

[11] A. Abimouloud, Behavior of a Partially Polluted Insulating Surface Under 50 Hz AC Voltage, Master's Thesis, Department of Electrical Engineering, National Polytechnic School (ENP), Algiers, December 1999.

[12] M. Teguar, A. Boubakeur, *Pollution of High Voltage Insulators*, 4th Year Course, Department of Electrical Engineering, ENP, Algiers.

[13] Z. Djemai, F. Bennai, On-Site and Laboratory Tests of Insulators Contaminated by Industrial Pollution on the Seaside, Final Year Project, Department of Electrical Engineering, ENP, Algiers, June 1986.

[14] M. Teguar, Mathematical Study of the Development Mechanisms of Electrical Discharges on Insulators Installed in Polluted Areas, Master's Thesis, Department of Electrical Engineering, ENP, Algiers, July 1993.

[15] M. Benakouche & R. Timghellette, *Behavior of an Insulator Model Under Impulse Voltage*, Final Year Project, Department of Electrical Engineering, ENP, Algiers, June 2005.
– A study on how insulator models respond to impulse voltages, relevant for understanding insulation performance under transient conditions.

[16] Quillet, *Encyclopedia of Industrial Sciences*, 1981.
– A general industrial science encyclopedia providing background knowledge on engineering and technical concepts.

[17] Fatiha Aouabed, *Contribution to the Study of an Equivalent Circuit of Synthetic Insulators Under Pollution Using EMTP*, Master's Thesis, Sétif, Algeria.

[18] Jean Ndoumbe, *Behavioral Study of Water Droplets Deposited on the Surface of a High Voltage Composite Insulator in the Presence of an Electric Field*, Doctoral School of Electronics, Electrical Engineering, and Automation of Lyon, École Centrale de Lyon, 2014.

[19] S. Zeraoulia, *Impact of Pollution on the Behavior of High Voltage Insulators in the Central Region of Algiers*, Master's Thesis, Department of Electrical Engineering, High Voltage Laboratory, National Polytechnic School of Algiers, 2007.

[20] Ravelomanantsoa, N. (2012). *Effect of Wind on the Pollution Accumulation Rate on the Surface of High Voltage Insulators in Winter Conditions*. Doctoral Thesis, University of Quebec at Chicoutimi.

[21] Fatiha Aouabed, *Contribution to the Study of an Equivalent Circuit of Synthetic Insulators Under Pollution Using EMTP*. Project Report, Ferhat Abbas University, Sétif, Algeria.

[22] Aouabed, F. *Contribution to the Study of an Equivalent Circuit of Synthetic Insulators Under Pollution Using EMTP*. Magister's Thesis, Ferhat Abbas University, Sétif.

[23] Bouzeroura, R. (2009). *Study of the Development of Parallel Electrical Arcs on a Non-Uniformly Polluted Insulating Surface Under DC Voltage*. Magister's Thesis, University of Bejaia.

[24] Khairoun, N., Abderrahmane, E., & Zellouta, D. (2008). *Tests on Polluted Insulators and Modeling*. Project Report, High Voltage Laboratory, National Polytechnic School of Algiers.
– A project report presenting experimental tests and modeling of polluted insulators under high voltage conditions.

[25] Sahli, Z. (*n.d.*). *Study of Pollution Non-Uniformity on the Breakdown Characteristics of Real Insulators Under DC Voltage*. Magister's Thesis, Department of Electrical Engineering, Abderrahmane Mira University of Bédjaia.

[26] Ben Alia, M. (2008). *Modeling of a Naturally Polluted Insulator Under Impulse Voltage Using Equivalent Electrical Circuits*. Magister's Thesis, High Voltage Laboratory, National Polytechnic School of Algiers.

[27] Slama, M. (2002). *Contribution to the Study of the Influence of Non-Uniform Pollution Based on the DDS Method for the Sizing of High Voltage AC Transmission Line Insulators*. Magister's Thesis, Mohamed Boudiaf University, Oran.

[28] Haddad, A., Waters, R., Griffiths, H., Chrzan, K., Harid, N., Sarkar, P., and Charalampidis, P., 'A new approach to anti-fog design for polymeric insulators', IEEE Trans. Dielectr. Electr. Insul., Vol. 17, (2): pp. 343-350, 2010

[29] Haddad, A. and Waters, R.T., Insulating Structures, UK Patent 2406225, 2003

[30] Albano, M., Charalampidis, P., Waters, R. T., Griffiths, H., & Haddad, A. (2014). *Silicone Rubber Insulators for Polluted Environments Part 2: Textured Insulators*. IEEE Transactions on Dielectrics and Electrical Insulation, 21(2), 749–757. https://doi.org/10.1109/TDEI.2013.004016

[31] Charalampidis, P., Albano, M., Griffiths, H., Haddad, A., & Waters, R. T. (2014). *Silicone Rubber Insulators for Polluted Environments Part 1: Enhanced Artificial Pollution Tests*. IEEE Transactions on Dielectrics and Electrical Insulation, 21(2), 740–748. https://doi.org/10.1109/TDEI.2013.004015

[32] IEC 60507: 1991: "Artificial pollution tests on high-voltage insulators to be used on a.c. systems" (currently under revision).

[33]Hani, T., Houba, A., & Messaoudi, S. (2024). *Surface Texturing of High Voltage Insulators: A Novel Approach for Performance Optimization*. Master's dissertation, University of Echahid Hamma Lakhdar - El Oued, Faculty of Technology, Department of Electrical Engineering.